Molecular Psychiatry (2014), 1–8

www.nature.com/mp

ORIGINAL ARTICLE

Evolutionarily conserved prefrontal-amygdalar dysfunction in early-life anxiety

RM Birn[1,2,3,4,5,12], AJ Shackman[6,7,8,12], JA Oler[2,3,4], LE Williams[2,3,4], DR McFarlin[2,3,4,5], GM Rogers[2], SE Shelton[2], AL Alexander[1,5], DS Pine[9], MJ Slattery[2], RJ Davidson[2,3,5,10,11], AS Fox[2,3,4,5,10,11] and NH Kalin[2,3,4,5,10]

Some individuals are endowed with a biology that renders them more reactive to novelty and potential threat. When extreme, this anxious temperament (AT) confers elevated risk for the development of anxiety, depression and substance abuse. These disorders are highly prevalent, debilitating and can be challenging to treat. The high-risk AT phenotype is expressed similarly in children and young monkeys and mechanistic work demonstrates that the central (Ce) nucleus of the amygdala is an important substrate. Although it is widely believed that the flow of information across the structural network connecting the Ce nucleus to other brain regions underlies primates' capacity for flexibly regulating anxiety, the functional architecture of this network has remained poorly understood. Here we used functional magnetic resonance imaging (fMRI) in anesthetized young monkeys and quietly resting children with anxiety disorders to identify an evolutionarily conserved pattern of functional connectivity relevant to early-life anxiety. Across primate species and levels of awareness, reduced functional connectivity between the dorsolateral prefrontal cortex, a region thought to play a central role in the control of cognition and emotion, and the Ce nucleus was associated with increased anxiety assessed outside the scanner. Importantly, high-resolution 18-fluorodeoxyglucose positron emission tomography imaging provided evidence that elevated Ce nucleus metabolism statistically mediates the association between prefrontal-amygdalar connectivity and elevated anxiety. These results provide new clues about the brain network underlying extreme early-life anxiety and set the stage for mechanistic work aimed at developing improved interventions for pediatric anxiety.

Molecular Psychiatry advance online publication, 27 May 2014; doi:10.1038/mp.2014.46

INTRODUCTION

Some children and animals characteristically show heightened reactions to novelty and potential threat.[1,2] When extreme, this anxious temperament (AT) is a well-established risk factor for the development of anxiety, depression and comorbid substance abuse.[3,4] These disorders are common, debilitating and difficult to treat.[5–7] As such, they represent a growing burden on public health-care systems and an important challenge for clinicians, health economists and public policy-makers.[8,9] AT is a trait-like phenotype that is determined by a combination of heritable and non-heritable factors, evident early in life and characterized by increased behavioral and hypothalamic–pituitary–adrenal reactivity to novelty and potential threat.[3,10–13] There is a considerable evidence that the high-risk AT phenotype is attenuated by anxiolytic compounds[14,15] and expressed similarly in children and young monkeys.[3,10] Importantly, mechanistic and neuroimaging studies in young monkeys demonstrate that metabolic activity in the central (Ce) nucleus of the amygdala is a key substrate for individual differences in early-life AT. In particular, selective excitotoxic lesions of the primate Ce nucleus reduce AT,[16] consistent with studies of human patients with circumscribed amygdala damage.[17] Furthermore, in young monkeys individual differences in Ce nucleus metabolism are trait-like and predict substantial variation in the AT phenotype.[10–13] These observations are in accord with evidence that the Ce nucleus can initiate a broad spectrum of defensive responses via efferent projections to the brain regions that directly mediate many of the behavioral, physiological and cognitive features of anxiety.[11,18,19]

There is consensus that neuropsychiatric disorders, like other complex mental processes, reflect alterations in the coordinated activity of distributed functional circuits.[20] Anatomically, the Ce nucleus is embedded in a complex web of monosynaptically and polysynaptically connected brain regions.[19] This structural backbone encompasses a number of cortical regions that are especially well developed in primates, including the anterior cingulate cortex (ACC), insula and prefrontal cortex (PFC).[21–23] Although it widely believed that the synchronized flow of information across this network underlies primates' capacity for flexibly regulating anxiety, the functional architecture of the Ce nucleus network and its relevance to early-life anxiety remains poorly understood. This partially reflects the fact that functional networks need not recapitulate the direct structural connections revealed by traditional tract tracing techniques.[24,25] In particular, there is mounting evidence that regulatory signals can propagate across more complex, indirect pathways.[26]

[1]Department of Medical Physics, University of Wisconsin, Madison, WI, USA; [2]Department of Psychiatry, University of Wisconsin, Madison, WI, USA; [3]HealthEmotions Research Institute, Wisconsin Psychiatric Institute and Clinics, University of Wisconsin, Madison, WI, USA; [4]Lane Neuroimaging Laboratory, University of Wisconsin, Madison, WI, USA; [5]Waisman Laboratory for Brain Imaging and Behavior, University of Wisconsin, Madison, WI, USA; [6]Department of Psychology, University of Maryland, College Park, MD, USA; [7]Neuroscience and Cognitive Science Program, University of Maryland, College Park, MD, USA; [8]Maryland Neuroimaging Center, University of Maryland, College Park, MD, USA; [9]Section on Development and Affective Neuroscience, National Institute of Mental Health, Bethesda, MD, USA; [10]Department of Psychology, University of Wisconsin, Madison, WI, USA and [11]Center for Investigating Healthy Minds, University of Wisconsin, Madison, WI, USA. Correspondence: Dr NH Kalin, HealthEmotions Research Institute, Wisconsin Psychiatric Institute and Clinics, University of Wisconsin, 6001 Research Park Boulevard, Madison, 53719 WI, USA.
E-mail: nkalin@wisc.edu
[12]These authors contributed equally to this work.
Received 5 January 2014; revised 7 March 2014; accepted 27 March 2014

Here, we used a combination of neuroimaging modalities to survey the entire brain for patterns of functional connectivity predictive of both the intermediate brain phenotype (Ce nucleus metabolism) and the high-risk phenotype (AT). Specifically, we used functional magnetic resonance imaging (fMRI) and high-resolution 18-fluorodeoxyglucose positron emission tomography (FDG-PET) to first trace the intrinsic functional connectivity of the Ce nucleus in anesthetized young monkeys and then to identify connectivity patterns associated with Ce nucleus metabolism and anxiety. fMRI-derived measures of intrinsic functional connectivity are particularly useful because they are sensitive to functional networks spanning polysynaptic circuits,[27–29] just as viral tracers can be used to delineate polysynaptic structural pathways.[30] Indeed, there is ample evidence of robust functional connectivity between brain regions that lack direct structural connections.[28,29,31] This is critical because the Ce nucleus is the major output region of the amygdala and receives relatively few direct projections from prefrontal regions implicated in the regulation of stress and anxiety.[19,32–34] Therefore, the regulation of Ce nucleus activity is likely to be mediated indirectly, via polysynaptic circuits spanning the PFC and neighboring regions of the amygdala with the capacity to convey cortical regulatory signals to the Ce nucleus.[19,32–33] Finally, to assess the relevance of our discoveries in the rhesus monkey to understanding childhood disease, we used fMRI to search for homologous patterns of intrinsic functional connectivity in children with anxiety disorders. Identifying an evolutionary conserved functional circuit relevant to extreme anxiety would reinforce the validity of the young rhesus model and set the stage for future mechanistic research aimed at understanding the origin of differences in the strength of functional connectivity.[35,36]

MATERIALS AND METHODS

Except where noted otherwise, behavioral and brain imaging methods have been described in detail in prior publications and are only briefly summarized.[10–13,37] Additional details are provided in the Supplementary Information.

Subjects

Young monkeys. Eighty-nine periadolescent monkeys (*Macaca mulatta*; median (*s.d.*) age = 2.69 (.97) years; 54% female) were phenotyped and brain imaged. This sample represents the subset of monkeys previously described by our group with complete multimodal imaging data sets (FDG-PET: $n = 238$; fMRI: $n = 107$).[11,12,37]

Children. Twenty-eight children (8–12 years) who met standard inclusion and exclusion criteria (see the Supplementary Information) were enrolled: 14 patients with a current pediatric anxiety disorder (mean age (s.d.) = 9.9 (1.2) years) and 14 demographically matched, psychiatrically healthy controls (mean age (s.d.) = 10.2 (1.3) years). Patients met criteria for one or more current pediatric anxiety disorders, including Generalized Anxiety Disorder, Separation Anxiety Disorder, Social Phobia or Anxiety Disorder Not Otherwise Specified. Children were recruited from local psychiatric clinics via clinician referral and from the community via media advertisements. The groups did not differ in age or sex (four females/group). Before the MRI scan, anxiety diagnoses were confirmed by a PhD-level clinical psychologist using the Kiddie-Schedule for Affective Disorders and Schizophrenia Present and Lifetime versions.[38] At the time of the MRI session, four patients were receiving psychotropic medications (see the Supplementary Information). Control children had no known history of mental illness (see the Supplementary Information).

Data acquisition and processing

Young monkeys. T1-weighted structural and T2*-weighted echoplanar imaging (EPI) functional MRI data were collected under anesthesia. As detailed in the Supplementary Information, EPI data were processed using standard techniques in AFNI (http://afni.nimh.nih.gov) except where noted otherwise. Data were processed to attenuate motion artifact, field distortions, physiological noise and slice-timing differences. To further attenuate physiological noise, average white matter and cerebrospinal fluid time series and their temporal derivatives were residualized from the EPI time series. EPI volumes with >1 mm of motion (see the Supplementary Information) were censored from data analyses. Using this criterion, no volumes were censored for any of the young monkeys.

In a separate session, monkeys received ^{18}FDG immediately before the 30-min No-Eye Contact challenge used to elicit the AT phenotype[10–13] (median (s.d.) intersession interval = 21.0 (42.4) days). Subjects were placed in a standard testing cage. An experimenter entered the room and stood motionless ~2.5 m from the subject while presenting his profile and avoiding direct eye contact. Subjects were allowed to freely respond to this ethologically relevant potential threat, similar to procedures used to assay dispositional anxiety and behavioral inhibition in children.[2–3] Increases in freezing and decreases in vocalizations were quantified by an experienced observer. Following behavioral testing, plasma was collected for quantifying cortisol and subjects were anesthetized and positioned in the PET scanner. Higher FDG-PET signals reflect greater regional metabolism (that is, increased FDG uptake) during the preceding No-Eye Contact challenge. FDG-PET, which provides a measure of regional brain metabolism integrated over the entire 30-min behavioral challenge, is ideally suited for assessing trait-like neural activity. AT was computed as the mean of standardized plasma cortisol, freezing and reverse-scored vocalizations in response to the human intruder's profile (30-min).

Children. Before scanning, children completed a mock MRI session, which has been shown to improve data quality in pediatric neuroimaging applications.[39] MRI data were collected using a standard eight-channel head coil. Anatomical scans were obtained with a 3D T1-weighted, inversion-recovery, fast gradient-echo prescription (inversion time/repetition time/echo time/flip angle/number of excitations/field of view/Matrix/Bandwidth: 450 ms/8.16 ms/3.18 ms/12°/1/256 mm/256 × 256/31.25 kHz) with whole-brain coverage (156 slices over 156 mm). Functional scans were obtained using a 2D T2*-weighted EPI prescription (inversion time/repetition time/echo time/flip angle/number of excitations/field of view/Matrix: 2000 ms/25 ms/60°/240 mm/64 × 64; 40 × 4.0-mm sagittal slices; gap: 0 mm; 180 volumes). Subjects were instructed to remain motionless while remaining relaxed and awake.

Except where noted otherwise, procedures were identical to those employed in the young nonhuman primate sample. Native-space T1 images were nonlinearly registered to the Montreal Neurological Institute probabilistic template (MNI152_T1_1 mm_brain; http://fsl.fmrib.ox.ac.uk) using FLIRT, FNIRT, and FSL.[40–42] Single-subject EPI data were spatially normalized using the resulting transformation matrices and re-sampled to 2-mm isotropic voxels. Normalized EPI data were spatially smoothed (6 mm full-width at half-maximum). Data sets were visually inspected to ensure adequate EPI coverage without excess susceptibility or distortion. The two groups did not significantly differ in the mean amount of motion or fraction of uncensored data, $Ps > .48$, $d.f. = 26$ (see the Supplementary Information).

Hypothesis testing

Young monkeys. A previously validated seed-based approach was used to identify the Ce nucleus functional network (see Supplementary Figure 1 and Supplementary Table 1 for additional validation analyses).[37] Given our focus on AT-related Ce nucleus metabolism, the seed was functionally defined as the 95% spatial confidence interval surrounding the Ce nucleus voxel, where FDG metabolism most strongly predicted AT in a superset of 238 individuals (turquoise region in Figure 1a; see Oler *et al.*[12]). Importantly, in prior work, we used *in vivo* chemoarchitectonic techniques to demonstrate that this functionally defined region corresponds to the sub-region of the primate amygdala where excitotoxic lesions attenuate anxiety,[12,16,37] a degree of precision that is difficult to achieve using conventional imaging techniques in humans (for example, see Herringa *et al.*[43] and Burghy *et al.*[44]). As in other recent work by our group,[43,44] hypothesis testing employed statistical maps that were thresholded ($P = .05$, corrected) based on cluster extent. Null distributions were estimated via Monte Carlo simulations (50 000 iterations; *3dClustSim*). Simulations incorporated the mean spatial smoothness of the single-subject residuals, estimated using *3dFWHMx*, and an uncorrected voxelwise threshold of $P = 0.005$. All hypothesis-testing analyses controlled for nuisance variation in mean-centered age and sex.

We used a standard multivariate analytic framework[45,46] to test whether the relationship between prefrontal-amygdalar functional connectivity and AT is statistically mediated by Ce nucleus metabolism (connectivity → metabolism → AT). As with our other analyses, we controlled for nuisance variance in mean-centered age and sex. For recent applications of this framework to neuroimaging data sets, see Shackman *et al.*, Lim *et al.* and

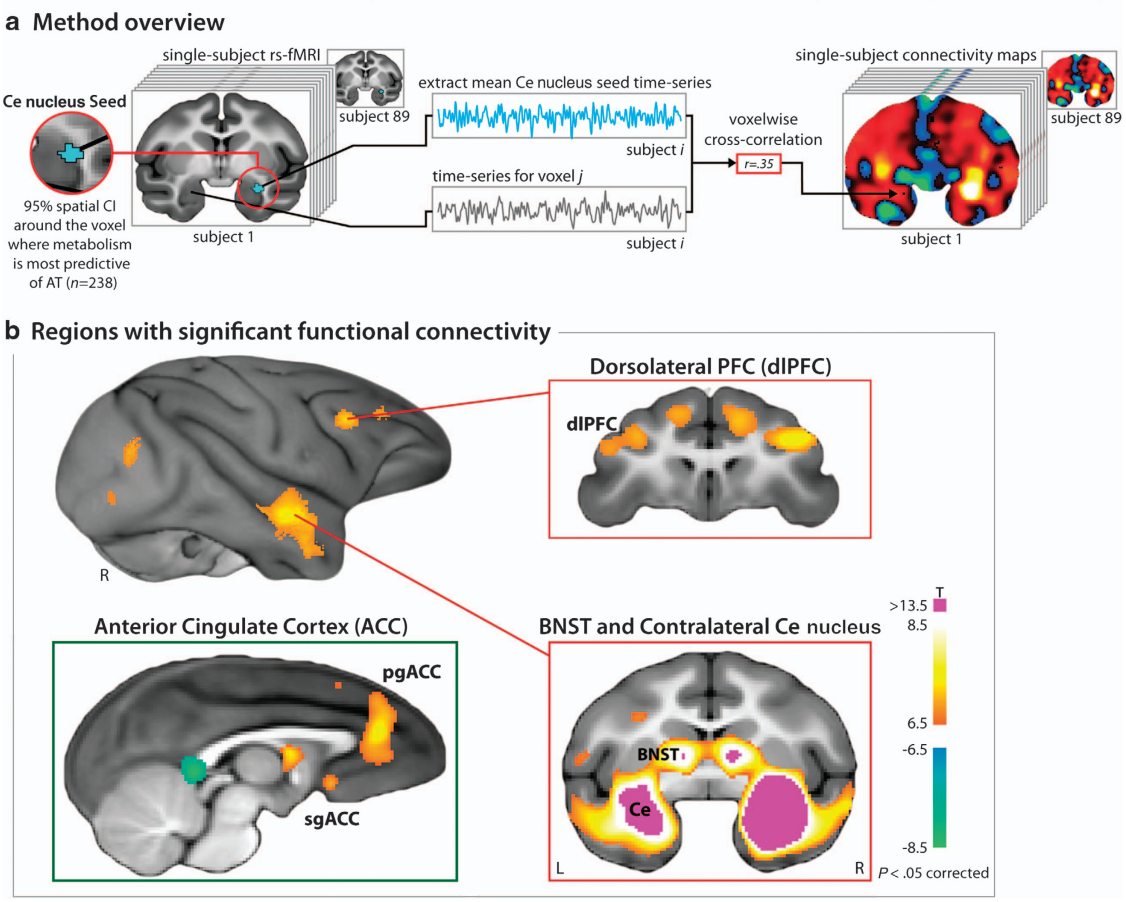

Figure 1. Intrinsic functional connectivity of the central (Ce) nucleus of the amygdala in young monkeys. (**a**) Method overview. The seed for functional connectivity analyses (depicted in turquoise) was functionally defined as the 95% spatial confidence interval (CI) surrounding the Ce nucleus voxel where fluorodeoxyglucose (FDG) metabolism best predicted individual differences in anxious temperament (AT) in a superset of 238 individuals (detailed in Oler *et al.*[12]). Using the mean de-noised echo planar imaging (EPI) time series from the seed (see the Materials and Methods and Supplementary Information), we computed voxelwise estimates of the strength of functional connectivity for each of the 89 individuals. (**b**) Regions with significant functional connectivity with the Ce nucleus. Significant ($P < 0.05$, corrected) clusters included the dorsolateral prefrontal cortex (dlPFC), pregenual anterior cingulate cortex (pgACC), subgenual ACC (sgACC), bed nucleus of the stria terminalis (BNST) and contralateral Ce nucleus. Red lines indicate the locations of the two coronal slices. L, left hemisphere; R, right hemisphere.

Wager *et al.*[11,47,48] Satisfying the criteria of this framework would demonstrate that a significant proportion of the association between prefrontal-Ce nucleus connectivity and AT is explained by metabolism, an inference not afforded by simpler bivariate tests. Operationally, mediation required four significant tests: (a) connectivity → metabolism, (b) connectivity → AT, (c) metabolism → AT and (d) controlling for variation in metabolism significantly weakens the connectivity → AT correlation. Consistent with our prior work,[11,49] the final criterion was assessed using Clogg's test[45,50] conservatively thresholded at $P < 0.05$ (Sidak-corrected for the total volume of the regions where connectivity predicted both Ce nucleus metabolism and AT; *d.f.* = *n*-3-number of covariates). Naturally, this test does not provide evidence of causation and more complex alternative pathways cannot be rejected.

Children. Imaging data were processed using the same techniques employed with the nonhuman primate sample. Here, the Ce nucleus seed was anatomically defined using well-established techniques (see the Supplementary Information).[37] Using this seed, we tested whether children with anxiety disorders and extremely anxious young monkeys show a similar pattern of Ce nucleus functional connectivity.

RESULTS

Young monkeys

Whole-brain regression analyses revealed several prefrontal and subcortical regions with significant Ce nucleus functional connectivity ($P < 5.0 \times 10^{-9}$, uncorrected; *d.f.* = 86; Figure 1b and Supplementary Table 2). These clusters encompassed regions that project to the Ce nucleus, such as the pregenual ACC, and regions that receive projections from the Ce nucleus, such as the bed nucleus of the stria terminalis.[19,32,37,51–53] Other clusters encompassed regions that appear to lack direction connections with the Ce nucleus, including the dorsolateral prefrontal cortex (dlPFC) and subgenual ACC.[19,32,37,51–53]

Next, we searched the entire brain for functional connections, indexed using fMRI, that are predictive of Ce nucleus metabolism, indexed using FDG-PET. This revealed that increased Ce nucleus metabolism was associated with decreased functional connectivity between the Ce nucleus and two prefrontal regions, mPFC and right dlPFC ($P < 0.05$, whole-brain corrected; *d.f.* = 85; Figure 2 and Supplementary Table 3). The mPFC cluster encompassed several architectonically distinct regions, including pregenual ACC (area 32), frontopolar cortex (area 10 M) and medial orbitofrontal cortex (OFC; area 14 M; see Supplementary Figure 2). Together, the dlPFC-Ce nucleus and mPFC-Ce nucleus functional networks statistically explained 22% of the variance in Ce nucleus metabolism ($F(2,84) = 5.92$, $P < 0.001$, uncorrected).

We also tested whether variation in intrinsic functional connectivity between these prefrontal regions and the Ce nucleus predicts AT. Paralleling the metabolism results (Figure 2), young

monkeys with higher levels of the anxious phenotype showed decreased functional connectivity between the Ce nucleus and both the medial and dorsolateral PFC clusters ($P < 0.05$, corrected; Figure 3a; Supplementary Table 4; Supplementary Figure 3). This indicates that functional connectivity measured under anesthesia is associated with objective differences in threat-elicited defensive behaviors and neuroendocrine activity assessed outside of the scanner environment. Exploratory analyses indicated that these relations were significant for each constituent of the composite AT phenotype (standardized freezing, vocalizations and cortisol: PRs = −0.25 to −0.32, uncorrected Ps < 0.03; $d.f. = 85$). Collectively, variation in the strength of connectivity between the Ce nucleus and these two prefrontal regions accounted for 23% of the variation in AT ($F(2,84) = 7.29$, $P < 0.001$, uncorrected).

Finally, we tested whether the association between prefrontal-Ce nucleus functional connectivity and the anxious phenotype is statistically mediated by Ce nucleus metabolic activity (that is, prefrontal-Ce nucleus connectivity → Ce nucleus metabolism → AT), as one would expect given evidence that the Ce nucleus is a mechanistically important proximal substrate of the anxious phenotype.[16] We first confirmed that Ce nucleus metabolism predicts AT in the present sample ($t = 6.70$, $P = 2.3 \times 10^{-9}$, uncorrected; $d.f. = 85$; Figure 3b), consistent with our prior report.[12] Critically, the statistical mediation test was also significant for both the dlPFC-Ce nucleus and mPFC-Ce nucleus networks, indicating that variation in Ce nucleus metabolism explains a significant proportion of the association between prefrontal-Ce nucleus functional connectivity and AT (Ps < .05, corrected; $d.f. = 84$; Figure 3c and Supplementary Figure 3, Supplementary Table 4). These effects were specific; control analyses demonstrated that mediation effects were not significant for alternative network models (that is, Ce nucleus metabolism → prefrontal-Ce nucleus connectivity → AT; ts < 2.52, Ps>0.05, corrected; $d.f. = 84$). Taken together, these findings are consistent with the possibility that the association between prefrontal-Ce nucleus functional connectivity (that is, mPFC-Ce nucleus and dlPFC-Ce nucleus) and dispositional anxiety reflects prefrontal influences on Ce nucleus metabolism, presumably supported by polysynaptic structural pathways. Importantly, control analyses indicated that individual differences in functional connectivity, Ce nucleus metabolism and AT were not significantly associated with variation in motion artifact, uncorrected Ps>0.24, $d.f. = 85$ (see the Supplementary Information).

Children

Our results indicate that young monkeys with extreme AT are characterized by decreased functional connectivity between the PFC and Ce nucleus under anesthesia. Next, we tested whether a similar pattern is evident in quietly resting children with anxiety disorders. In fact, patients showed decreased functional connectivity between the dlPFC and Ce nucleus compared with healthy control subjects ($P < 0.05$, when corrected for the combined volume of the dlPFC and mPFC; $d.f. = 24$; n.s. when corrected for the volume of the entire brain; Figure 4a,

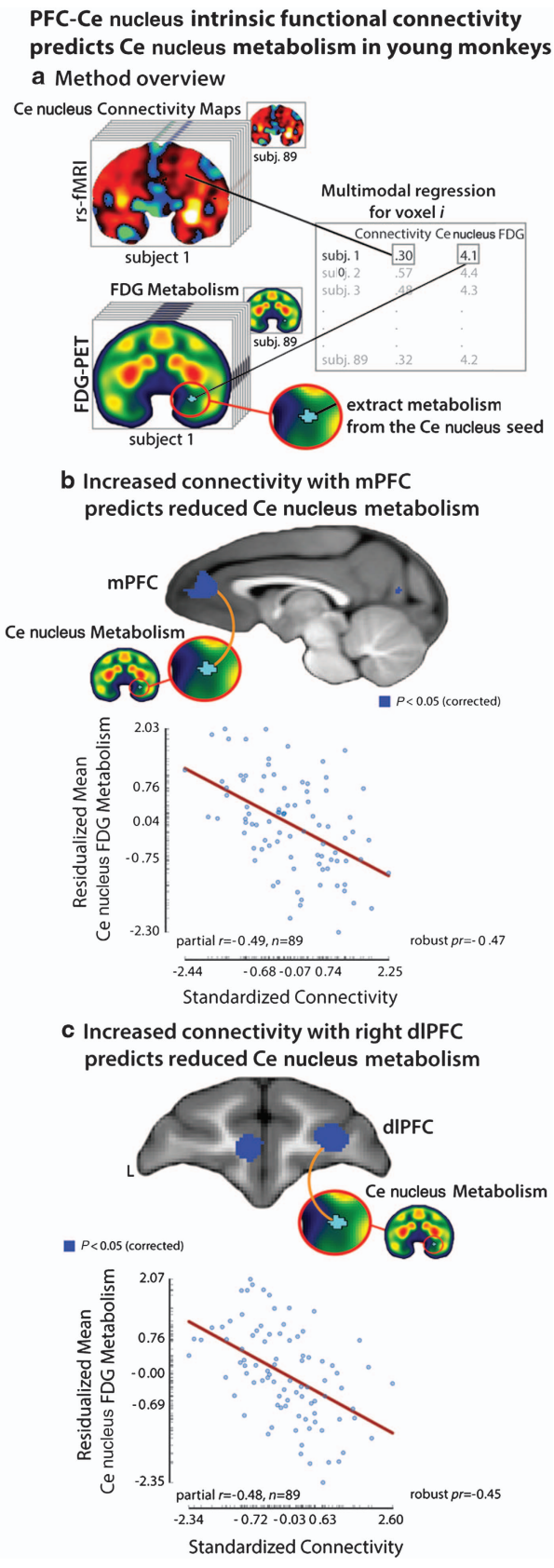

Figure 2. Prefrontal cortex (PFC)-central (Ce) nucleus intrinsic functional connectivity predicts Ce nucleus metabolism in young monkeys. (**a**) Method overview. For each monkey, a Ce nucleus functional connectivity map was computed and the mean level of fluorodeoxyglucose (FDG) metabolism was extracted from the Ce nucleus seed (turquoise region). Individual differences in Ce nucleus metabolism were used to predict voxelwise functional connectivity with the Ce nucleus throughout the brain. (**b**) Decreased functional connectivity with the medial PFC (mPFC) predicts increased Ce nucleus metabolism. (**c**) Decreased functional connectivity with the right dorsolateral PFC (dlPFC) predicts increased Ce nucleus metabolism. For illustrative purposes, scatter plots depict the partial correlations between connectivity and metabolism for the cluster averages. Axis labels indicate the minimum, maximum and interquartile range. Partial correlation coefficients were computed using robust regression techniques[11] are shown to the right of each scatter plot. PET, positron emission tomography.

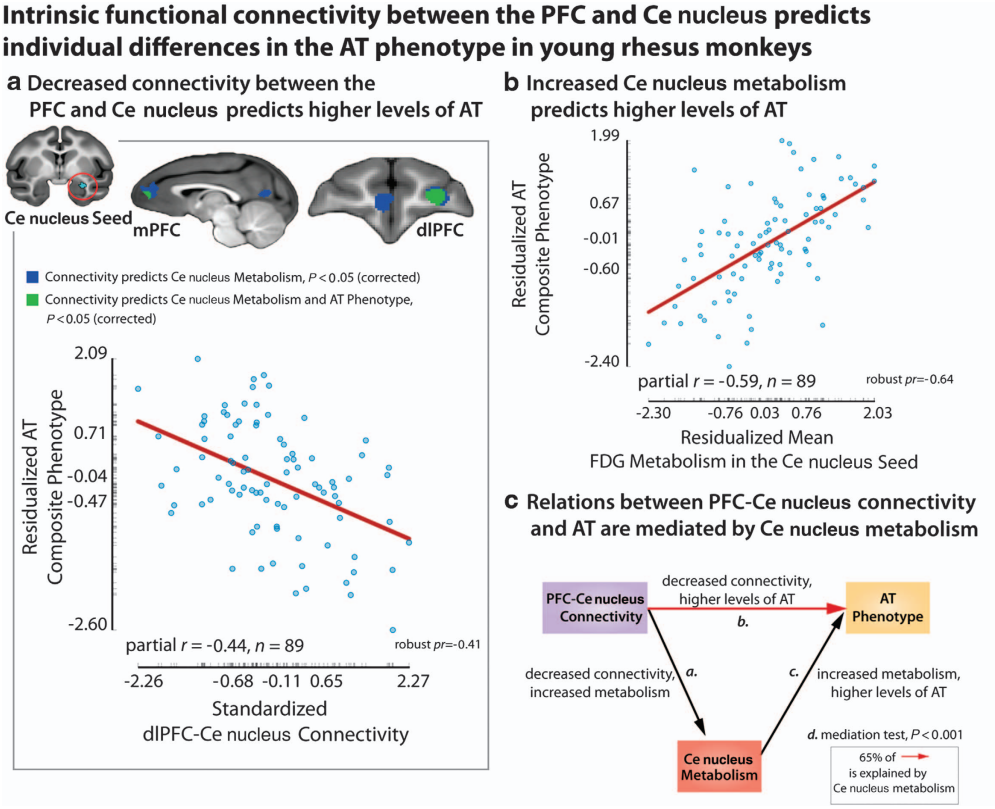

Figure 3. Intrinsic functional connectivity between the prefrontal cortex (PFC) and central (Ce) nucleus predicts individual differences in the anxious temperament (AT) phenotype in young rhesus monkeys. (**a**) Decreased connectivity between the PFC and Ce nucleus predicts higher levels of AT. Upper panel depicts the regions within the medial PFC (mPFC) and dorsolateral PFC (dlPFC) clusters where the strength of functional connectivity significantly predicted variation in both Ce nucleus metabolism and AT (displayed in green; $P < 0.05$, corrected). Lower panel shows the partial correlation between dlPFC-Ce nucleus connectivity and AT (controlling for age and sex). (**b**) Increased Ce nucleus metabolism predicts higher levels of AT. (**c**) Relations between PFC-Ce nucleus connectivity and AT are significantly mediated by Ce nucleus metabolism. Summary of the four tests (*a*–*d*) incorporated in the multivariate mediation framework (see the Supplementary Information). For scatter plot conventions, see Figure 3. Panel depicts results for the dlPFC. Similar results were obtained for the mPFC (see Supplementary Table 4).

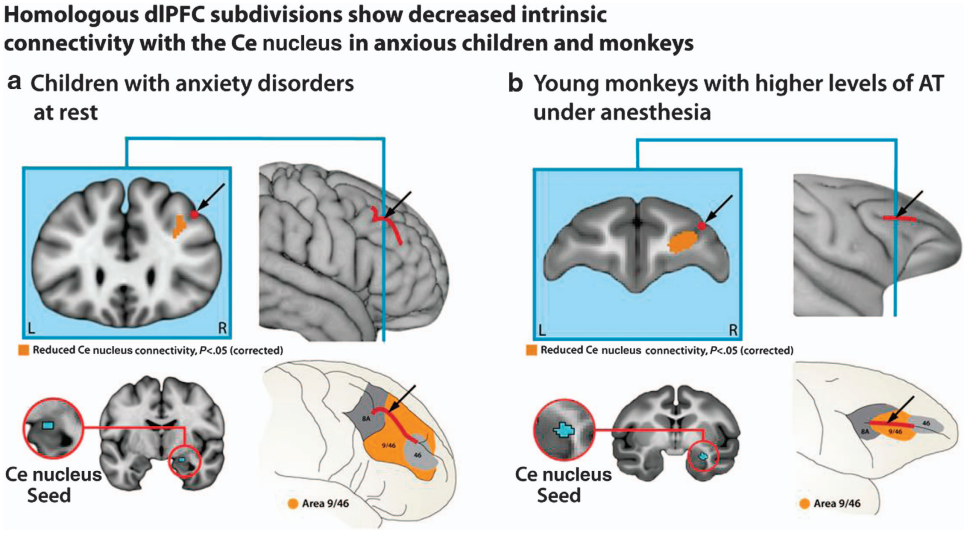

Figure 4. Homologous dorsolateral prefrontal cortex (dlPFC) subdivisions show decreased intrinsic connectivity with the central (Ce) nucleus in anxious children and monkeys. (**a**) Children with anxiety disorders at rest. Bottom-left panel shows the Ce nucleus seed (cyan in red ring). Upper-left panel depicts a coronal slice through the human dlPFC cluster (dark orange; $P < 0.05$, corrected for the combined volume of the mPFC and right dlPFC; n.s. when corrected for the volume of the whole brain). The intermediate frontal sulcus (IFS) is shown in dark red. Upper-right panel shows the IFS with the location of the coronal slice indicated by the blue vertical line. Bottom-right panel shows the location of the dlPFC cluster relative to the architectonic subdivisions of the human dlPFC. (**b**) Young monkeys with high levels of anxious temperament (AT) under anesthesia. Conventions are similar to **a**; dark red indicates the location of the sulcus principalis. The bottom-right panels of this figure were adapted with permission from Badre and D'Esposito.[74] L, left hemisphere; R, right hemisphere.

Supplementary Figures 5 and 6, and Supplementary Table 5). Significant effects were not obtained for the mPFC-Ce nucleus network in the pediatric anxiety sample. Accordingly, in the remainder of the report we focus on the evolutionarily conserved dlPFC-Ce nucleus functional network. Follow-up analyses revealed that the reduction in dlPFC-Ce nucleus connectivity evident in the pediatric patients remained significant after controlling for age and sex (Supplementary Table 5), controlling for individual differences in motion (see the Supplementary Information) or excluding four medicated patients (see the Supplementary Information). Collectively, these results demonstrate that decreased functional connectivity between the dlPFC and Ce nucleus is associated with extreme anxiety outside the imaging environment in both quietly resting children and anesthetized young monkeys (Figures 4a and b). The consistency of this relationship across species and levels of awareness at the time of scanning makes it unlikely that it reflects either a sedation artifact or differences in stress elicited by the scanner environment.

DISCUSSION

The present results provide evidence that extreme anxiety early in life is associated with evolutionarily conserved alterations in the strength of intrinsic functional connectivity between the dlPFC and Ce nucleus. Among both children and monkeys, individuals with low levels of connectivity were characterized by high levels of anxiety when assessed outside of the scanner environment (Figures 2 and 4), raising the possibility that chronically altered functional coordination between these regions contributes to the development of pathological anxiety. In the larger sample of young monkeys, decreased functional connectivity with the dlPFC as well as the mPFC was associated with elevated metabolism in the Ce nucleus, a mechanistically important substrate for trait-like differences in anxiety.[12,16]

In children, AT is a well-established risk factor for the development of anxiety and other psychiatric disorders[3,4] and our results provide a novel framework for understanding the mechanisms underlying this liability. Prior work suggests that Ce nucleus metabolism underlies much of the experience-dependent risk that contributes to the development of extreme anxiety.[12,13] Likewise, recent work suggests that prefrontal-amygdalar functional connectivity can be influenced by early adversity.[43,44] This plasticity suggests that interventions targeting either Ce nucleus metabolism or the larger functional circuit in which it is embedded may prove to be effective strategies for reducing anxiety in children who, because of their extreme temperament, are at increased risk for developing psychopathology. By virtue of its well-established capacity for regulating mood, attention, memory and action,[34,54–56] the dlPFC is well positioned to translate early-life experiences into enduring alterations in Ce nucleus function.

Given the absence of established direct projections, the association between dlPFC-Ce nucleus functional connectivity and early-life anxiety is presumably supported by a polysynaptic structural network. Although our results do not identify the precise constituents of this circuit, there is growing mechanistic evidence that the PFC can influence information processing in distal brain regions via biasing signals that propagate across polysynaptic structural pathways.[26,57,58] This network could reflect either undiscovered projections[59,60] or established projections from the dlPFC to neighboring regions of the dorsal amygdala, such as the magnocellular division of the basal nucleus, that are strongly interconnected with the Ce nucleus. In particular, the dlPFC projects to a dorsal region of the basal nucleus that lies within a few millimeters of the Ce,[19,51–53] a difference that cannot be resolved using conventional fMRI techniques (see the Supplementary Information).

Analyses of data obtained from the larger nonhuman primate sample revealed that Ce nucleus metabolism statistically mediates the association between prefrontal-amygdalar connectivity and AT, suggesting that Ce nucleus metabolic activity represents an intermediate link between intrinsic functional connectivity and chronically elevated anxiety (that is, decreased prefrontal-Ce nucleus connectivity → increased Ce nucleus metabolism → increased anxiety; Figure 3). Notably, this pattern was evident for functional connectivity between the Ce nucleus and two regions of the PFC: dlPFC and mPFC. Although our results do not provide evidence that the mPFC-Ce nucleus is evolutionarily conserved, this may simply reflect insufficient power in the pediatric anxiety sample. Other work highlights the potential importance of the mPFC-Ce nucleus functional network. For example, reduced functional connectivity between the mPFC and amygdala has been shown to predict heightened dispositional anxiety in several human imaging studies.[59,60] The present results suggest that this association between connectivity and anxiety stems from chronically elevated metabolic activity in the Ce nucleus.

Clearly, important challenges remain. As with other brain imaging studies, our analyses do not permit mechanistic inferences and alternative causal pathways are possible. Like other studies focused on measures of functional connectivity, our conclusions are tempered by questions about the origins and significance of correlated fluctuations in the blood oxygen level-dependent fMRI signal.[61–63] Furthermore, although it is clear from lesion studies that the Ce nucleus is mechanistically involved in AT,[16] we cannot reject the possibility that both increased anxiety and reduced prefrontal functional connectivity reflect symptoms of chronically elevated Ce nucleus metabolism. In particular, the Ce nucleus is well positioned to influence the signal-to-noise ratio of information processing in the PFC,[64–67] via projections to diffuse neuromodulatory systems in the basal forebrain and striatum. Dampened prefrontal signal-to-noise ratio would manifest as reduced functional connectivity.[68] A key challenge for future studies will be to use mechanistic techniques in nonhuman primates to adjudicate between these alternatives and to more fully delineate the polysynaptic circuit supporting correlated activity in the dlPFC and Ce nucleus. Combined with fMRI, transcranial magnetic stimulation represents a noninvasive alternative strategy that could be applied in humans.[69,70] It will also be important to test whether existing anxiolytic compounds rescue dlPFC-Ce nucleus functional connectivity. If so, then this biomarker could potentially be used to evaluate novel therapeutics.[36,71] Finally, it will be useful to more fully evaluate whether aberrant dlPFC-Ce nucleus functional connectivity is a transdiagnostic feature of the anxiety disorders and whether it represents a substrate for childhood AT or related constructs, such as behavioral inhibition and shyness, that were not assessed in the pediatric sample.

CONCLUSIONS

Existing treatments for anxiety disorders are inconsistently effective or associated with significant adverse effects,[5,7] highlighting the need to identify and understand the neural mechanisms that confer risk. Building on prior mechanistic and neuroimaging work, the present study demonstrates that extreme anxiety is associated with reduced functional connectivity between the dlPFC and Ce nucleus in anesthetized young monkeys and quietly resting children. Translational brain imaging strategies, like that featured in the present report, provide a powerful tool for closing the gap separating the mechanistic insights afforded by nonhuman animal models from the complexity of human psychopathology and accelerating the pace of therapeutic development.[35–36] Our results also indicate that the association between prefrontal-amygdalar connectivity and anxiety is statistically mediated by Ce nucleus metabolism. Importantly, these results are fundamentally grounded in psychiatrically important emotional behaviors. For example, differences in the strength of prefrontal-Ce nucleus functional connectivity were found to predict anxiety-related behaviors (that is, behavioral inhibition) and cortisol elicited by an

ethologically relevant threat in freely behaving young monkeys. The use of a relatively large discovery sample, functionally and mechanistically defined seed region, well-validated primate model of pediatric anxiety and clinical confirmatory sample enhances confidence in the translational significance of these results.[72] More broadly, the present study provides unique evidence that early-life temperament does not just reflect differences in neural reactivity to trait-relevant cues (for example, the amygdala's threshold to respond or peak response to threat[2,73]), but is also embodied in the intrinsic activity of the brain.

CONFLICT OF INTEREST

The authors declare no conflict of interest.

ACKNOWLEDGMENTS

We acknowledge the assistance of E Ahlers, V Balchen, B Christian, A Converse, L Friedman, M Jesson, E Larson, K Mayer, T Oakes, M Riedel, P Roseboom, J Storey, D Tromp, N Vack, H Van Valkenberg and the staffs of the Harlow Center for Biological Psychology, HealthEmotions Research Institute (HERI), Waisman Center, Waisman Laboratory for Brain Imaging and Behavior and Wisconsin National Primate Center. We thank Julie Fudge, Luiz Pessoa, and several anonymous reviewers for critical feedback. This work was supported by the National Institutes of Health (NIH; Intramural Research Program and extramural grants HD003352, HD008352, MH018931, MH046729, MH081884, MH084051, MH090912, MH091550, OD011106 and RR000167), HERI, Meriter Hospital and the University of Maryland.

AUTHOR CONTRIBUTIONS

NHK, JAO, DSP, MJS and SES designed the study. SES collected monkey data. LEW collected human data. ALA optimized imaging methods. DSP, NHK and GMR made childhood psychiatric diagnoses. RMB and ASF developed analytical tools. RMB, JAO, AJS and ASF performed data processing for monkey data. DRM, LEW, JAO, AJS and RMB performed data processing for human data. RMB, AJS, JAO and NHK analyzed monkey data. DRM, LEW, JAO, AJS, RMB and NHK analyzed human data. AJS, NHK, RMB, ASF, JAO, RJD and DSP interpreted data. AJS, ASF, NHK, JAO, LEW and RMB wrote the paper. AJS, ASF and NHK created the figures. AJS, JAO and LEW created the tables. NHK supervised the study. All authors contributed to revising the paper.

REFERENCES

1 Darwin C. *The Expression of the Emotions in Man and Animals*. 4th edn. Oxford University Press: NY, 1872/2009.
2 Kagan J, Reznick JS, Snidman N. Biological bases of childhood shyness. *Science* 1988; **240**: 167–171.
3 Fox NA, Henderson HA, Marshall PJ, Nichols KE, Ghera MM. Behavioral inhibition: linking biology and behavior within a developmental framework. *Annu Rev Psychol* 2005; **56**: 235–262.
4 Blackford JU, Pine DS. Neural substrates of childhood anxiety disorders: a review of neuroimaging findings. *Child Adolesc Psychiatr Clin N Am* 2012; **21**: 501–525.
5 Bystritsky A. Treatment-resistant anxiety disorders. *Mol Psychiatry* 2006; **11**: 805–814.
6 Kessler RC, Petukhova M, Sampson NA, Zaslavsky AM, Wittchen HU. Twelve-month and lifetime prevalence and lifetime morbid risk of anxiety and mood disorders in the United States. *Int J Methods Psychiatr Res* 2012; **21**: 169–184.
7 Cloos JM, Ferreira V. Current use of benzodiazepines in anxiety disorders. *Curr Opin Psychiatry* 2009; **22**: 90–95.
8 Collins PY, Patel V, Joestl SS, March D, Insel TR, Daar AS *et al.* Grand challenges in global mental health. *Nature* 2011; **475**: 27–30.
9 Whiteford HA, Degenhardt L, Rehm J, Baxter AJ, Ferrari AJ, Erskine HE *et al.* Global burden of disease attributable to mental and substance use disorders: findings from the Global Burden of Disease Study 2010. *Lancet* 2013; **382**: 1575–1586.
10 Fox AS, Shelton SE, Oakes TR, Davidson RJ, Kalin NH. Trait-like brain activity during adolescence predicts anxious temperament in primates. *PLoS OneNE* 2008; **3**: e2570.
11 Shackman AJ, Fox AS, Oler JA, Shelton SE, Davidson RJ, Kalin NH. Neural mechanisms underlying heterogeneity in the presentation of anxious temperament. *Proc Natl Acad Sci USA* 2013; **110**: 6145–6150.
12 Oler JA, Fox AS, Shelton SE, Rogers J, Dyer TD, Davidson RJ *et al.* Amygdalar and hippocampal substrates of anxious temperament differ in their heritability. *Nature* 2010; **466**: 864–868.
13 Fox AS, Oler JA, Shelton SE, Nanda SA, Davidson RJ, Roseboom PH *et al.* Central amygdala nucleus (Ce) gene expression linked to increased trait-like Ce metabolism and anxious temperament in young primates. *Proc Natl Acad Sci USA* 2012; **109**: 18108–18113.
14 Kalin NH, Shelton SE, Turner JG. Effects of alprazolam on fear-related behavioral, hormonal, and catecholamine responses in infant rhesus monkeys. *Life Sci* 1991; **49**: 2031–2044.
15 Kalin NH, Shelton SE. Defensive behaviors in infant rhesus monkeys: environmental cues and neurochemical regulation. *Science* 1989; **243**: 1718–1721.
16 Kalin NH, Shelton SE, Davidson RJ. The role of the central nucleus of the amygdala in mediating fear and anxiety in the primate. *J Neurosci* 2004; **24**: 5506–5515.
17 Feinstein JS, Adolphs R, Damasio A, Tranel D. The human amygdala and the induction and experience of fear. *Curr Biol* 2011; **21**: 1–5.
18 Pare D, Duvarci S. Amygdala microcircuits mediating fear expression and extinction. *Curr Opin Neurobiol* 2012; **22**: 717–723.
19 Freese JL, Amaral DG. Neuroanatomy of the primate amygdala. In: Whalen PJ, Phelps EA (eds). *The human amygdala*. Guilford: NY, 2009, pp 3–42.
20 Uhlhaas PJ, Singer W. Neuronal dynamics and neuropsychiatric disorders: toward a translational paradigm for dysfunctional large-scale networks. *Neuron* 2012; **75**: 963–980.
21 Shackman AJ, Salomons TV, Slagter HA, Fox AS, Winter JJ, Davidson RJ. The integration of negative affect, pain and cognitive control in the cingulate cortex. *Nat Rev Neurosci* 2011; **12**: 154–167.
22 Preuss TM. Primate brain evolution in phylogenetic context. In: Kaas JH, Preuss TM (eds). *Evolution of Nervous Systems* vol. 4. Elsevier: NY, 2007, pp 3–34.
23 Ongur D, Price JL. The organization of networks within the orbital and medial prefrontal cortex of rats, monkeys and humans. *Cereb Cortex* 2000; **10**: 206–219.
24 Pessoa L. *The Cognitive-Emotional Brain: From Interactions to Integration*. MIT Press: Cambridge, MA, 2013.
25 Pessoa L. Beyond brain regions: network perspective of cognition-emotion interactions. *Behav Brain Sci* 2012; **35**: 158–159.
26 Ekstrom LB, Roelfsema PR, Arsenault JT, Bonmassar G, Vanduffel W. Bottom-up dependent gating of frontal signals in early visual cortex. *Science* 2008; **321**: 414–417.
27 Buckner RL, Krienen FM, Yeo BT. Opportunities and limitations of intrinsic functional connectivity MRI. *Nat Neurosci* 2013; **16**: 832–837.
28 Vincent JL, Patel GH, Fox MD, Snyder AZ, Baker JT, Van Essen DC *et al.* Intrinsic functional architecture in the anaesthetized monkey brain. *Nature* 2007; **447**: 83–86.
29 Honey CJ, Sporns O, Cammoun L, Gigandet X, Thiran JP, Meuli R *et al.* Predicting human resting-state functional connectivity from structural connectivity. *Proc Natl Acad Sci USA* 2009; **106**: 2035–2040.
30 Dum RP, Levinthal DJ, Strick PL. The spinothalamic system targets motor and sensory areas in the cerebral cortex of monkeys. *J Neurosci* 2009; **29**: 14223–14235.
31 Adachi Y, Osada T, Sporns O, Watanabe T, Matsui T, Miyamoto K *et al.* Functional connectivity between anatomically unconnected areas is shaped by collective network-level effects in the macaque cortex. *Cereb Cortex* 2012; **22**: 1586–1592.
32 Ghashghaei HT, Barbas H. Pathways for emotion: interactions of prefrontal and anterior temporal pathways in the amygdala of the rhesus monkey. *Neuroscience* 2002; **115**: 1261–1279.
33 Stefanacci L, Amaral DG. Some observations on cortical inputs to the macaque monkey amygdala: an anterograde tracing study. *J Comp Neurol* 2002; **451**: 301–323.
34 Buhle JT, Silvers JA, Wager TD, Lopez R, Onyemekwu C, Kober H *et al.* Cognitive reappraisal of emotion: A meta-analysis of human neuroimaging studies. *Cereb Cortex* 2013 (in press).
35 Casey BJ, Craddock N, Cuthbert BN, Hyman SE, Lee FS, Ressler KJ. DSM-5 and RDoC: progress in psychiatry research? *Nat Rev Neurosci* 2013; **14**: 810–814.
36 Borsook D, Becerra L, Hargreaves R. A role for fMRI in optimizing CNS drug development. *Nat Rev Drug Discov* 2006; **5**: 411–424.
37 Oler JA, Birn RM, Patriat R, Fox AS, Shelton SE, Burghy CA *et al.* Evidence for coordinated functional activity within the extended amygdala of non-human and human primates. *Neuroimage* 2012; **61**: 1059–1066.
38 Kaufman J, Birmaher B, Brent D, Rao U, Flynn C, Moreci P *et al.* Schedule for Affective Disorders and Schizophrenia for School-Age Children-Present and Lifetime Version (K-SADS-PL): initial reliability and validity data. *J Am Acad Child Adolesc Psychiatry* 1997; **36**: 980–988.
39 deBie HM, Boersma M, Wattjes MP, Adriaanse S, Vermeulen RJ, Oostrom KJ *et al.* Preparing children with a mock scanner training protocol results in high quality structural and functional MRI scans. *Eur J Pediatr* 2010; **169**: 1079–1085.
40 Smith SM, Jenkinson M, Woolrich MW, Beckmann CF, Behrens TE, Johansen-Berg H *et al.* Advances in functional and structural MR image analysis and implementation as FSL. *Neuroimage* 2004; **23**: S208–S219.

41 Woolrich MW, Jbabdi S, Patenaude B, Chappell M, Makni S, Behrens T *et al.* Bayesian analysis of neuroimaging data in FSL. *Neuroimage* 2009; **45**: S173–S186.
42 Zhang Y, Brady M, Smith S. Segmentation of brain MR images through a hidden Markov random field model and the expectation-maximization algorithm. *IEEE Trans Med Imaging* 2001; **20**: 45–57.
43 Herringa RJ, Birn RM, Ruttle PL, Burghy CA, Stodola DE, Davidson RJ *et al.* Childhood maltreatment is associated with altered fear circuitry and increased internalizing symptoms by late adolescence. *Proc Natl Acad Sci USA* 2013; **110**: 19119–19124.
44 Burghy CA, Stodola DE, Ruttle PL, Molloy EK, Armstrong JM, Oler JA *et al.* Developmental pathways to amygdala-prefrontal function and internalizing symptoms in adolescence. *Nat Neurosci* 2012; **15**: 1736–1741.
45 MacKinnon DP, Lockwood CM, Hoffman JM, West SG, Sheets V. A comparison of methods to test mediation and other intervening variable effects. *Psychol Methods* 2002; **7**: 83–104.
46 Baron RM, Kenny DA. The moderator-mediator variable distinction in social psychological research: Conceptual, strategic, and statistical considerations. *J Pers Soc Psychol* 1986; **51**: 1173–1182.
47 Lim SL, Padmala S, Pessoa L. Segregating the significant from the mundane on a moment-to-moment basis via direct and indirect amygdala contributions. *Proc Natl Acad Sci USA* 2009; **106**: 16841–16846.
48 Wager TD, Davidson ML, Hughes BL, Lindquist MA, Ochsner KN. Prefrontal-subcortical pathways mediating successful emotion regulation. *Neuron* 2008; **59**: 1037–1050.
49 Shackman JE, Shackman AJ, Pollak SD. Physical abuse amplifies attention to threat and increases anxiety in children. *Emotion* 2007; **7**: 838–852.
50 Clogg CC, Petkova E, Shihadeh ES. Statistical methods for analyzing collapsibility in regression models. *J Educ Stat* 1992; **17**: 51–74.
51 Barbas H, De Olmos J. Projections from the amygdala to basoventral and mediodorsal prefrontal regions in the rhesus monkey. *J Comp Neurol* 1990; **300**: 549–571.
52 Amaral DG, Insausti R. Retrograde transport of D-[3 H]-aspartate injected into the monkey amygdaloid complex. *Exp Brain Res* 1992; **88**: 375–388.
53 Amaral DG, Price JL. Amygdalo-cortical projections in the monkey (*Macaca fascicularis*). *J Comp Neurol* 1984; **230**: 465–496.
54 Miller EK, Cohen JD. An integrative theory of prefrontal cortex function. *Annu Rev Neurosci* 2001; **24**: 167–202.
55 Shackman AJ, McMenamin BW, Maxwell JS, Greischar LL, Davidson RJ. Right dorsolateral prefrontal cortical activity and behavioral inhibition. *Psychol Sci* 2009; **20**: 1500–1506.
56 Koenigs M, Huey ED, Calamia M, Raymont V, Tranel D, Grafman J. Distinct regions of prefrontal cortex mediate resistance and vulnerability to depression. *J Neurosci* 2008; **28**: 12341–12348.
57 Ekstrom LB, Roelfsema PR, Arsenault JT, Kolster H, Vanduffel W. Modulation of the contrast response function by electrical microstimulation of the macaque frontal eye field. *J Neurosci* 2009; **29**: 10683–10694.
58 Premereur E, Janssen P, Vanduffel W. FEF-microstimulation causes task-dependent modulation of occipital fMRI activity. *Neuroimage* 2012; **67**: 42–50.
59 Pezawas L, Meyer-Lindenberg A, Drabant EM, Verchinski BA, Munoz KE, Kolachana BS *et al.* 5-HTTLPR polymorphism impacts human cingulate-amygdala interactions: a genetic susceptibility mechanism for depression. *Nat Neurosci* 2005; **8**: 828–834.
60 Kim MJ, Gee DG, Loucks RA, Davis FC, Whalen PJ. Anxiety dissociates dorsal and ventral medial prefrontal cortex functional connectivity with the amygdala at rest. *Cereb Cortex* 2011; **7**: 1667–1673.
61 Akam T, Kullmann DM. Oscillatory multiplexing of population codes for selective communication in the mammalian brain. *Nat Rev Neurosci* 2014; **15**: 111–122.
62 Cabral J, Kringelbach ML, Deco G. Exploring the network dynamics underlying brain activity during rest. *Prog Neurobiol* 2014; **114C**: 102–131.
63 Logothetis NK. What we can do and what we cannot do with fMRI. *Nature* 2008; **453**: 869–878.
64 Arnsten AF. Stress signalling pathways that impair prefrontal cortex structure and function. *Nat Rev Neurosci* 2009; **10**: 410–422.
65 Shackman AJ, Maxwell JS, McMenamin BW, Greischar LL, Davidson RJ. Stress potentiates early and attenuates late stages of visual processing. *J Neurosci* 2011; **31**: 1156–1161.
66 Davis M, Whalen PJ. The amygdala: vigilance and emotion. *Mol Psychiatry* 2001; **6**: 13–34.
67 Fudge JL, Haber SN. The central nucleus of the amygdala projection to dopamine subpopulations in primates. *Neuroscience* 2000; **97**: 479–494.
68 Fornito A, Harrison BJ, Goodby E, Dean A, Ooi C, Nathan PJ *et al.* Functional dysconnectivity of corticostriatal circuitry as a risk phenotype for psychosis. *JAMA Psychiatry* 2013; **70**: 1143–1151.
69 Guller Y, Ferrarelli F, Shackman AJ, Sarasso S, Peterson MJ, Langheim FJ *et al.* Probing thalamic integrity in schizophrenia using concurrent transcranial magnetic stimulation and functional magnetic resonance imaging. *Arch Gen Psychiatry* 2012; **69**: 662–671.
70 Chen AC, Oathes DJ, Chang C, Bradley T, Zhou ZW, Williams LM *et al.* Causal interactions between fronto-parietal central executive and default-mode networks in humans. *Proc Natl Acad Sci USA* 2013; **110**: 19944–19949.
71 Bullmore E. The future of functional MRI in clinical medicine. *Neuroimage* 2012; **62**: 1267–1271.
72 Button KS, Ioannidis JP, Mokrysz C, Nosek BA, Flint J, Robinson ES *et al.* Power failure: why small sample size undermines the reliability of neuroscience. *Nat Rev Neurosci* 2013; **14**: 365–376.
73 Davidson RJ. Affective style and affective disorders: perspectives from affective neuroscience. *Cogn Emot* 1998; **12**: 307–330.
74 Badre D, D'Esposito M. Is the rostro-caudal axis of the frontal lobe hierarchical? *Nat Rev Neurosci* 2009; **10**: 659–669.

Supplementary Information accompanies the paper on the Molecular Psychiatry website (http://www.nature.com/mp)

Supplementary Information (SI) to Accompany

RM Birn, AJ Shackman, JA Oler, LE Williams, DR McFarlin, GM Rogers, SE Shelton, AL Alexander, DS Pine, MJ Slattery, RJ Davidson, AS Fox & NH Kalin

Address Correspondence to:
Ned H. Kalin (nkalin@wisc.edu), HealthEmotions Research Institute, Wisconsin Psychiatric Institute & Clinics, University of Wisconsin—Madison, 6001 Research Park Boulevard, Madison, Wisconsin 53719 USA

SUPPLEMENTARY METHOD AND RESULTS FOR THE YOUNG MONKEYS STUDY

Quantifying Individual Differences in the AT Phenotype

Anxiety-related behaviors elicited by the NEC challenge were unobtrusively quantified by a well-trained rater using a closed-circuit audio-visual system. Freezing was defined as a period of >3-seconds characterized by a tense body posture and the absence of vocalizations or movements other than slow head movements or eye-blinks. 'Coo' calls are contact or separation vocalizations that are elicited by exposure to the test cage (i.e., the 'alone' condition of the HIP) and suppressed by exposure to the NEC challenge (i.e., human intruder's profile)[1-4]. Coo vocalizations were defined as audible calls characterized by an increase then decrease in frequency and intensity made by rounding and pursing the lips. Mean freezing duration and cooing frequency were $\log_e$ and square-root transformed, respectively. Plasma cortisol (μg/dL) was quantified in duplicate using the DPC Coat-a-count radioimmunoassay (Siemens, Los Angeles, CA). Assaying procedures were highly reliable (inter-assay CV=6.6%; intra-assay CV=4.0%) and sensitive (lower detection limit=1 μg/dL). Standardized cortisol, freezing, and vocalization measures were created by linearly removing nuisance variance in age and, in the case of cortisol, time-of-day using SPSS (version 21; IBM Inc., Armonk, NY)[5-8]. The AT composite phenotype was computed as the arithmetic mean of standardized cortisol, freezing, and vocalization[6]; vocalizations were first reflected (-1 × standardized coo frequency) to ensure that larger values indicated increased reactivity to the NEC challenge.

FDG-PET

Subjects were deeply anesthetized (15mg/kg ketamine i.m.), intubated, and positioned in a stereotactic device within the Siemens/Concorde microPET P4 scanner[9]. Both FDG and attenuation scans were acquired. Metabolism during the PET scan reflects the amount of FDG uptake during the preceding behavioral paradigm; regions that are more metabolically active during the NEC challenge take up more radio-labeled

glucose. General anesthesia was maintained using 1-2% isoflurane gas. Images were reconstructed using standard filtered-backprojection techniques with attenuation- and scatter-correction.

MRI

MRI data were collected under anesthesia using a General Electric (GE) SIGNA 3T MRI scanner (GE Healthcare, Waukesha, WI) equipped with a 16-cm quadrature extremity coil. Subjects were anesthetized with ketamine (15 mg/kg i.m.), placed in a stereotactic head-frame integrated with the coil, fit with a standard GE pulse oximeter and pneumatic respiration belt, and positioned in the scanner. Immediately prior to the start of the first scan, subjects received medetomidine (30 µg/kg i.m.). Small doses of ketamine were administered as needed to maintain anesthesia (<15 mg/kg). Heart rate and respiration were recorded using the pulse oximeter and respiration belt, respectively. Anatomical scans were obtained with a 3D T1-weighted, inversion-recovery, fast gradient echo prescription (TI/TR/TE/Flip/NEX/FOV/Matrix/Bandwidth: 600ms/8.65ms/1.89ms/10°/2/140mm/256×224/61.1 kHz) with whole brain coverage (128 slice encodes over 128 mm) reconstructed to 0.27×0.27×0.5 mm on the scanner). Functional scans were obtained using a 2D T2*-weighted echo-planar image (EPI) prescription (TR/TE/Flip/FOV/Matrix: 2500ms/25ms/90°/140mm/64×64; 26×3.1-mm axial slices; gap: 0.5-mm; 360 volumes).

Processing Pipeline

Prior to spatial normalization, brains were manually extracted from T1 images using SPAMALIZE (http://psyphz.psych.wisc.edu/~oakes/spam/spam_frames.htm). Native-space, brain-extracted T1 images were linearly registered (12-*df*) to a pre-existing in-house macaque template[6] in the stereotactic space of Paxinos and colleagues[10] using FLIRT (http://fsl.fmrib.ox.ac.uk/fsl/flirt). Images were visually inspected and averaged to create an age-appropriate, study-specific linear template (0.625-mm^3). Native-space, brain-extracted T1 images were then nonlinearly registered to the template using FNIRT

(http://www.fmrib.ox.ac.uk/fsl/fnirt) and segmented into gray matter (GM), white matter (WM), and cerebrospinal fluid (CSF) probability maps using FAST (http://www.fmrib.ox.ac.uk/fsl/fast4). In the accompanying figures, functional data are shown superimposed on the mean T1 image (*n*=89). Some figures were created using MRIcron (http://www.mccauslandcenter.sc.edu/mricro/mricron).

Single-subject PET images were linearly registered to the corresponding native-space T1 images (6-*df*). The resulting transformation matrices were concatenated with those defining the nonlinear transformation to the template and used to spatially normalize the PET images. Normalized PET images were global-mean scaled within the brain using SPAMALIZE. Scaled PET and GM probability maps were spatially smoothed (4mm FWHM Gaussian).

EPI data were processed using standard techniques[11-14] in AFNI (http://afni.nimh.nih.gov)[15] except where noted otherwise. The initial three time points were removed and data were processed to attenuate motion artifact (6-*df*), B_0-field distortions (PRELUDE: http://www.fmrib.ox.ac.uk/fsl/fugue/prelude.html; http://brainimaging.waisman.wisc.edu/~jjo/fieldmap_correction/make_fmap.html), physiological noise[16], and slice-timing differences. Single-subject, native-space, brain-extracted T1 images were linearly registered to the corresponding EPI images, allowing only for shifts within the coronal plane[17]. The resulting transformation matrix was reversed, concatenated with the other transform matrices (see above), and used to normalize the EPI data to the rhesus MRI template (interpolated to 0.625-mm^3).

To further attenuate physiological noise, average WM and CSF time-series and their temporal derivatives were residualized from the EPI time series[18]. WM and CSF regions were identified by thresholding segmented T1 images. To minimize contributions from adjacent GM regions, WM was eroded by 2 voxels and CSF was limited to the lateral ventricles by multiplying single-subject CSF regions by a template-defined mask.

Artifact-attenuated EPI data were spatially (4mm FWHM Gaussian) and temporally (0.01- 0.1Hz) filtered. We visually verified that all datasets showed adequate EPI coverage without excess susceptibility or distortion artifacts (e.g., signal shearing or compression). Quantitatively, we verified that all datasets showed adequate temporal signal-to-noise ratio (tSNR = mean/variance > 100) in regions vulnerable to susceptibility artifacts (e.g., orbitofrontal and medial temporal cortices)[19, 20]. EPI volumes with >1mm of volume-to-volume motion were censored from data analyses. As in our prior work[21], 'motion' was defined to include estimated displacements (x, y, z) and rotations (a, b, c) over time (t) in the three cardinal planes: $((x_t - x_{t-1})^2 + (y_t - y_{t-1})^2 + (z_t - z_{t-1})^2 + (a_t - a_{t-1})^2 + (b_t - b_{t-1})^2 + (c_t - c_{t-1})^2)^{-1/2}$. Using this criterion, no volumes were censored for any of the young monkeys.

Quantifying Intrinsic Functional Connectivity

Given our aims, we adopted a standard *a priori* seed-based approach to quantifying intrinsic functional connectivity[12-14, 22-24]. Seed regions are described below. For each subject, we performed a voxelwise correlation between the artifact-attenuated EPI time-series, averaged across the voxels defining the seed, and voxel times-series throughout the brain. Correlation maps were normalized (Fisher's *R*-to-*Z* transformation) and used to identify regions with consistent functional connectivity across subjects. This was done by testing the intercept in a regression model controlling for mean-centered age and sex, equivalent to a single-sample *t* test (*df*=86).

Quality Assurance Analyses of the Default Mode Resting-State Network (DM-RSN)

For quality assurance purposes, we performed a confirmatory analysis of the DM-RSN. This network—typically including regions of the posterior cingulate cortex (PCC), dorsomedial prefrontal cortex (dmPFC), and lateral temporoparietal cortex—is among the most commonly assessed and reproducible RSNs in humans[25] and monkeys[26]. Using a PCC seed (adapted from Ref. [24]), we performed a whole-brain connectivity analysis.

The resulting map was conservatively thresholded ($|t|>16.0$, $p<1.6 \times 10^{-27}$, uncorrected) to maximize correspondence with prior reports employing small samples. Confirming the integrity of our approach, the topography of the DM-RSN closely resembled prior observations in the rhesus monkey[24, 26] (**Fig. S1 and Table S1**).

Assessing Motion Artifact in the Young Nonhuman Primate Study

Control analyses (*df*=85; controlling for mean-centered age and sex; uncorrected *p*-values) indicated that motion was not significantly correlated with variation in the AT phenotype (*r*=-.13, *p*=.25), Ce FDG metabolism (*r*=-.08, *p*=.45), dlPFC-Ce functional connectivity (*r*=.05, *p*=.64), or dmPFC-Ce (*r*=.01, *p*=.90) functional connectivity. This indicates that our results cannot be explained by subtle individual differences in motion artifact.

Signal-to-Noise Ratio (SNR) Control Analyses

Functional connectivity is a complex metric that reflects the influence of several variables, including the degree of regional coupling and temporal SNR (i.e., 'shot-to-shot' SNR)[27, 28]. To assess whether our conclusions in young monkeys were primarily due to variation in regional signal quality, we recomputed the mediation tests controlling for temporal SNR (i.e., the mean divided by the standard deviation of the time-series)[20] in both the Ce seed and the prefrontal clusters. The mediation test remained similarly strong in the mPFC and dlPFC (*t*s<-5.22, *p*s<.05, Sidak-corrected, *df*=84) indicating that our inferences about functional connectivity cannot be explained by individual differences in signal quality.

SUPPLEMENTARY METHOD AND RESULTS FOR THE PEDIATRIC ANXIETY STUDY

Subjects

Inclusion criteria included age (8-12 years), ability to speak and understand English, and ability to lie motionless in the scanner for 45 minutes. Exclusion criteria included: current psychosis or suicidal ideation; or a lifetime history of autism, bipolar disorder, dyslexia, fetal alcohol syndrome, obsessive-compulsive disorder, phenylketonuria, schizophrenia; or an acute/ unstable medical illness; or a chronic medical illness requiring medication; or participation in a study involving an investigational drug in the last 30 days; or MRI incompatibility (e.g., implanted medical devices). All patients met KSADS-PL criteria for one or more current DSM-IV-TR[29] pediatric anxiety disorders, including Generalized Anxiety Disorder (GAD; *n*=9), Separation Anxiety Disorder (*n*=4), Social Phobia (*n*=7), Specific Phobia (*n*=1), or Anxiety Disorder Not Otherwise Specified (*n*=2). Twelves of the fourteen patients received two or more diagnoses. Comorbid diagnoses included another anxiety disorder (*n*=9), major depressive disorder (*n*=3), attention-deficit/hyperactivity disorder (ADHD; *n*=3), and oppositional defiant disorder (ODD; *n*=2). Most of the children received a diagnosis of GAD and/or Social Phobia (*n*=11). At the time of the MRI session, 4 patients were receiving psychotropic medications to stabilize mood (*n*=2, fluoxetine) or treat ADHD (*n*=1, atomoxetine; *n*=1, methylphenidate). Control children had no history of mental illness based on parental responses to a verbal interview that assessed the presence of a number of disorders (e.g., ADHD, anxiety, bipolar, depressive, eating, learning/pervasive developmental, ODD, psychotic, and substance abuse).

Processing Pipeline for the Pediatric Anxiety Study

Data acquisition parameters are described in the main report. Except where noted otherwise, data reduction and analytic procedures were identical to those employed in the young nonhuman primate sample.

Assessing Motion Artifact in the Pediatric Anxiety Study

Patients (mean (SD) = .18 mm (.18)) and controls (mean (SD) = .15 mm (.11)) did not significantly differ in the mean amount of motion, t=.49, p=.63, df=26. Likewise, patients (mean (SD) = 97.1% (5.6%)) and controls

(mean (SD) = 98.3% (3.5%)) did not significantly differ in the percentage-of-uncensored data, t=-.71, p=.48, df=26.

Anatomically Defining the Ce Seed in Children

The Ce seed for the pediatric functional connectivity analysis was anatomically defined using techniques similar to those previously described by our group[14]. Here, the location of the Ce region-of-interest (ROI) was manually prescribed by one of the authors (J.A.O.) using the same probabilistic template employed in the nonlinear spatial normalization. Visual inspection indicated that, when combined with nonlinear spatial normalization, this approach provided enhanced anatomical sensitivity and selectivity compared to the probabilistic 'centromedial' amygdala ROI distributed with the FSL software package[30]. The Ce ROI prescription was derived from Ref. [31] (see **Fig. 4** in the main report and **Fig. S4**). The ROI began 4 mm caudal to the rostral margin of the amygdala and continued in the caudal direction for 8 mm. The rostral portion of the ROI was prescribed ventral and medial to the lateral extension of the anterior commissure (AC; i.e., where the AC converges with the uncinate fasciculus). Throughout, the ROI was prescribed lateral to the optic tract and dorsal to the temporal horn of the lateral ventricle. The Ce seed was generated by spatially smoothing (1-voxel dilation, followed by 1-voxel erosion) and decimating (2-mm) the ROI. Using the spatially-normalized T1, we manually verified that the seed was centered on and the peak voxel in the single-subject functional connectivity map was located within the provisional location of the Ce for each child.

Confirmatory Testing in Children: Assessing the translational importance of the dlPFC-Ce and mPFC-Ce functional networks

Our analyses demonstrate that young monkeys with extreme AT are characterized by decreased functional connectivity between the dlPFC/mPFC and the Ce. To assess whether this dysfunctional pattern of intrinsic connectivity is evolutionarily conserved, we tested whether children suffering from pediatric anxiety disorders show a homologous decrease in the intrinsic functional connectivity of the Ce with the medial

and/or dorsolateral PFC compared to psychiatrically-healthy control children. Specifically, we computed a between-groups *t*-test, thresholded at $p<.05$ ($df=26$), corrected for the combined volume of the right dlPFC and mPFC using the same Monte Carlo technique we employed in the young monkey analyses (**Fig. S5**). The location and extent of the ROIs was dictated by our results in the juvenile rhesus sample. The total volume of these two regions in the human template (22,256 mm^3) was computed by summing the extent of the right dlPFC (i.e., middle frontal gyrus rostral to the slice where the caudate and putamen are present in both hemispheres) and bilateral mPFC (i.e., anterior division of the cingulate gyrus and paracingulate gyrus below the dorsal border of the corpus callosum and 8 mm rostral to the genu of the corpus callosum) masks in the Harvard-Oxford probabilistic atlas distributed with FSL (>25% probability; HarvardOxford-cort-maxprob-thr25-2mm.nii). Several follow-up analyses were conducted. In particular, we re-computed the *t*-test while controlling for nuisance variance in mean-centered age and sex separately for each group ($p<.05$, corrected). For descriptive purposes, we also extracted mean connectivity from the right dlPFC cluster and re-computed the *t*-test after excluding the 4 medicated patients. The decrease in dlPFC-Ce connectivity observed in the complete pediatric sample ($t=4.00$, $p<.001$ uncorrected, $df=26$) remained significant in the medication-free sample ($t=3.62$, $p=.002$ uncorrected, $df=22$). Likewise, the decrease in dlPFC-Ce connectivity observed in the complete pediatric sample remained significant after controlling for individual differences in mean-centered motion (Group: $t=4.09$, $p<.001$ uncorrected, $df=25$; Motion: $t=1.16$, $p=.29$ uncorrected, $df=25$) or percentage-of-uncensored data (Group: $t=4.17$, $p<.001$ uncorrected, $df=25$; Percentage Data: $t=1.51$, $p=.23$ uncorrected, $df=25$), confirming that our results were not driven by subtle differences in motion.

A Note on Structural and Functional Connectivity

We suggest that the dlPFC-Ce functional network could reflect a dlPFC-Bmc-Ce structural pathway. In particular, we note that the dlPFC projects to a region of the dorsal Bmc that lies within a few millimeters of the Ce[32-35]. While these modest projections are sometimes characterized as “weak,” recent mechanistic work

indicating that numerically modest structural projections can support robust functional connectivity[36]. This is in accord with other kinds of evidence demonstrating that modest structural projections can have profound consequences for brain function. For example, lateral geniculate nucleus (LGN) lesions are sufficient to produce blindness and abolish visual responses in primary visual cortex (V1), despite the fact that direct LGN-V1 connections constitute less than 10% of all V1 afferents[37]. Taken with evidence that the Ce and Bmc are densely interconnected[35], the possibility exists that the dlPFC-Ce functional network that we identified is anatomically supported by a dlPFC-Bmc-Ce structural pathway.

Continued…

SUPPLEMENTARY FIGURES AND LEGENDS

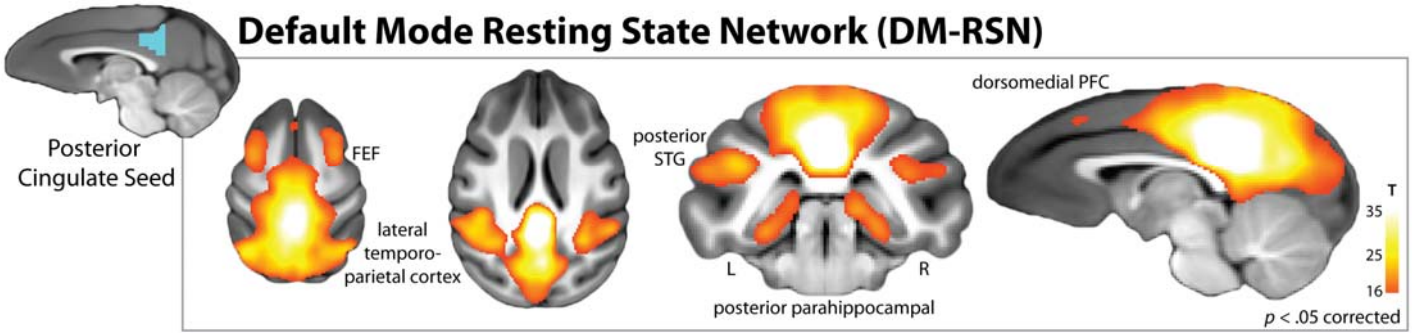

Fig. S1. The macaque homolog to the default mode resting state network (DM-RSN). The topography of the network closely resembles prior observations in small samples (*n*s < 12) of anesthetized macaques. Inset shows the posterior cingulate seed (turquoise) used in this analysis (adapted from Ref. [24]). The underlying brain is the average of the 89 spatially-normalized T1-weighted MRIs. **Abbreviations—FEF:** frontal eye fields (area 8 in the vicinity of the arcuate sulcus); **L:** left hemisphere; **PFC:** prefrontal cortex; **R:** right hemisphere; **STG:** superior temporal gyrus.

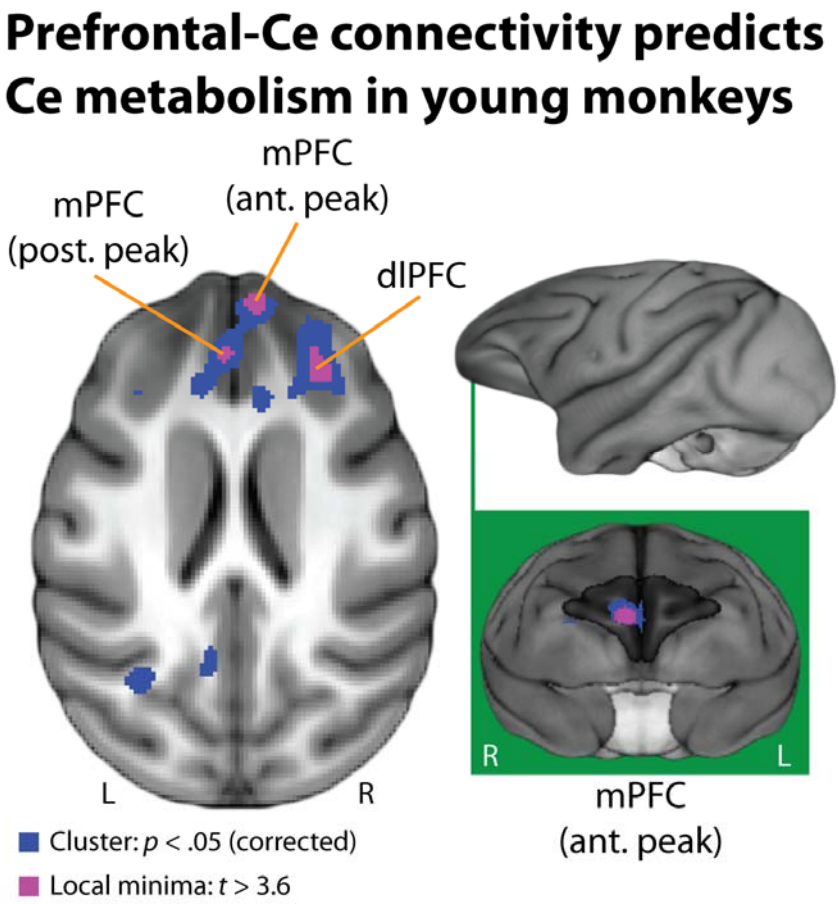

Fig. S2. Prefrontal-Ce connectivity predicts Ce metabolism in young monkeys. Left: Figure depicts local minima (negative peaks; shown in purple) for the regression in which voxelwise functional connectivity was used to predict Ce metabolism. This revealed several regions, including the dorsolateral PFC (dlPFC) and medial PFC (mPFC). The mPFC cluster spanned two local minima: a posterior (post.) peak in the left pregenual anterior cingulate cortex (pgACC) and an anterior (ant.) peak in the vicinity of the right rostral sulcus. **Right:** Green line indicates the location of a coronal slice through the anterior mPFC peak, which lies at the intersection of the frontopolar cortex (area 10M), gyrus rectus (area 14M), and rostral sulcus principalis (area 46). Brain is the mean of 89 normalized T1-weighted images. **L:** left; **R:** right.

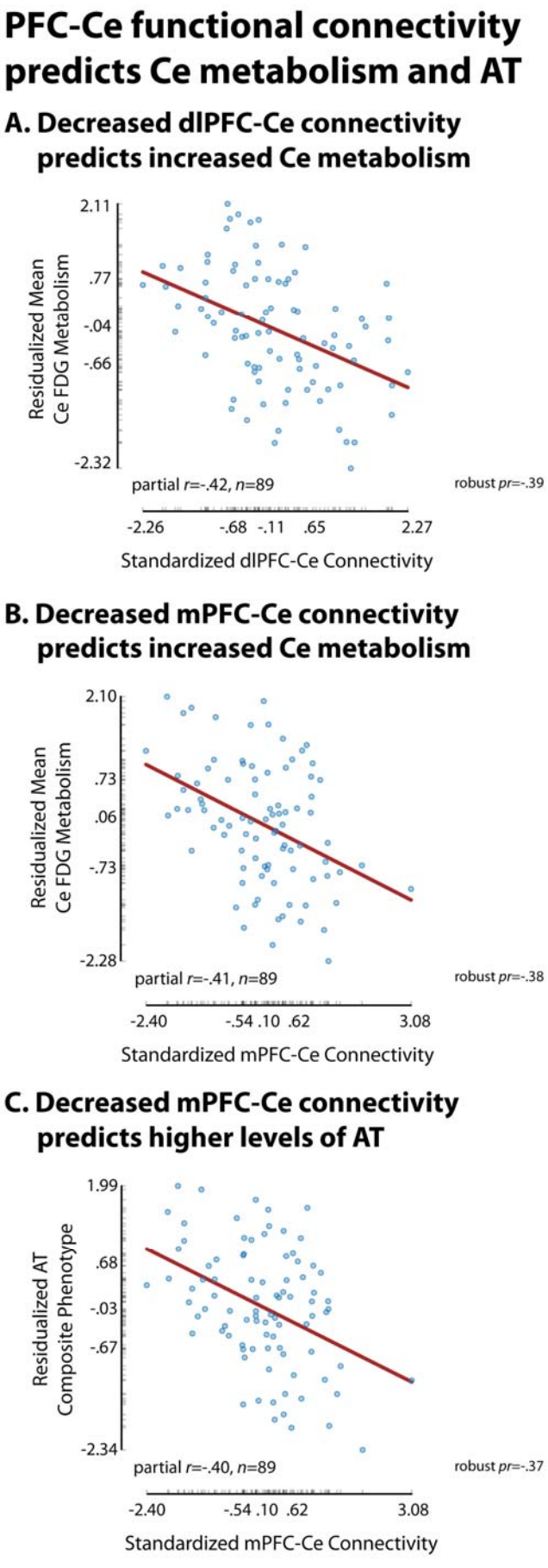

Fig. S3. Scatterplots for prefrontal regions where the strength of intrinsic functional connectivity with the Ce significantly predicts variation in Ce metabolism and AT in young monkeys. For illustrative purposes, scatter plots depict the partial correlations between functional connectivity and metabolism for the cluster averages. The prefrontal regions are depicted in green in Fig. 3a in the main report. Regressions controlled for nuisance variation in mean-centered age and sex. Axis labels indicate the minimum, maximum, and interquartile range (25th, 50th, and 75th percentiles). Partial correlation coefficients computed using an alternative robust regression technique[8] are shown to the right of each scatter plot.

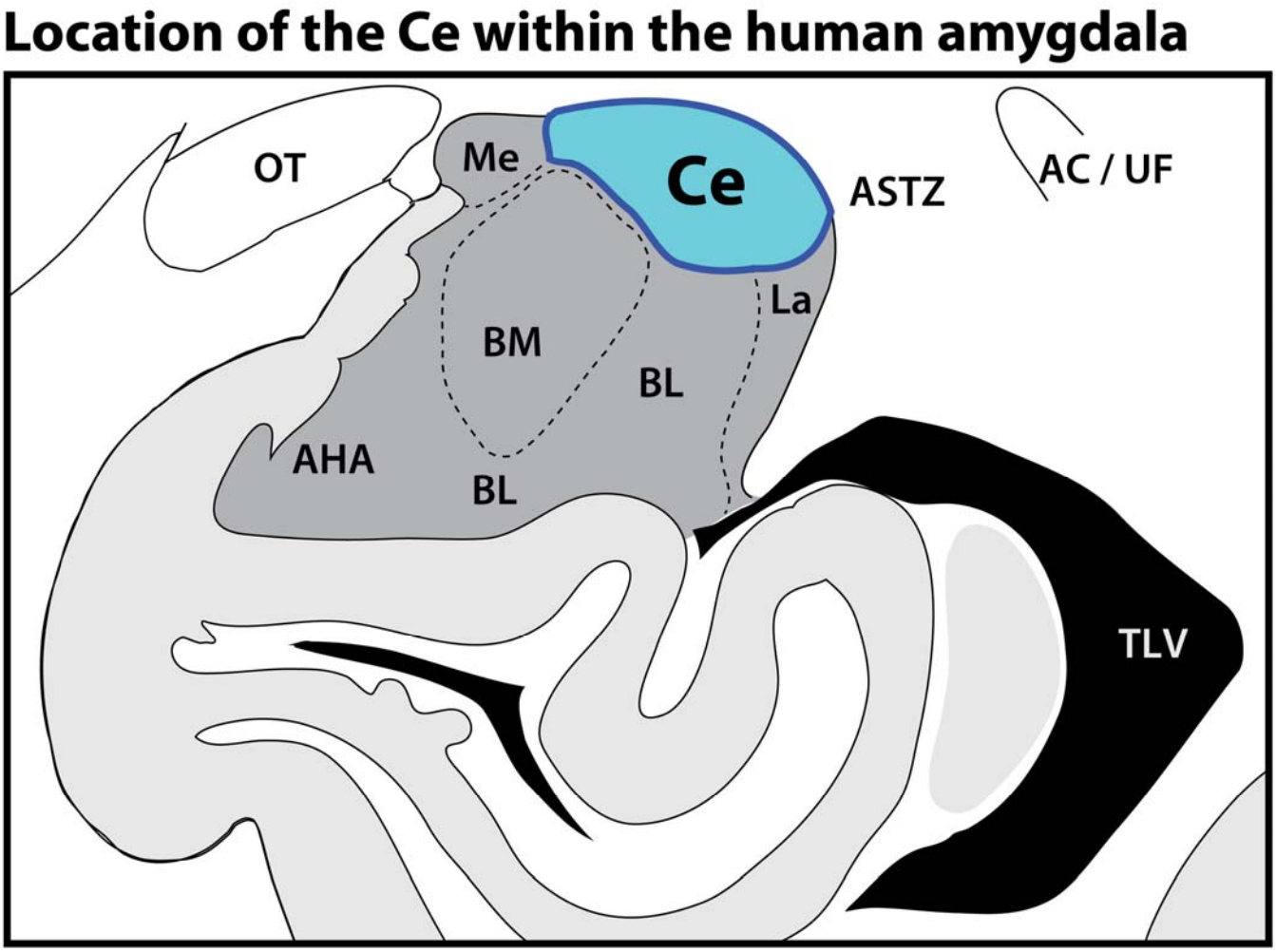

Fig. S4. The location of the central nucleus (Ce) in the human amygdala. In this simplified schematic, the Ce is shown in turquoise, other amygdalar nuclei are shown in dark gray, the cortex and hippocampus are shown in light gray, and ventricular cerebrospinal fluid is shown in black. Figure was adapted with permission from Ref. [31]. Abbreviations—**AC:** anterior commissure; **AHA:** amygdalo-hippocampal area; **ASTZ:** amygdalo-striatal transition area; **BL:** basolateral nucleus; **BM:** basomedial nucleus; **Ce:** central nucleus; **La:** lateral nucleus; **Me:** medial nucleus; **OT:** optic tract; **TLV:** temporal horn of the lateral ventricle; **UF:** uncinate fasciculus.

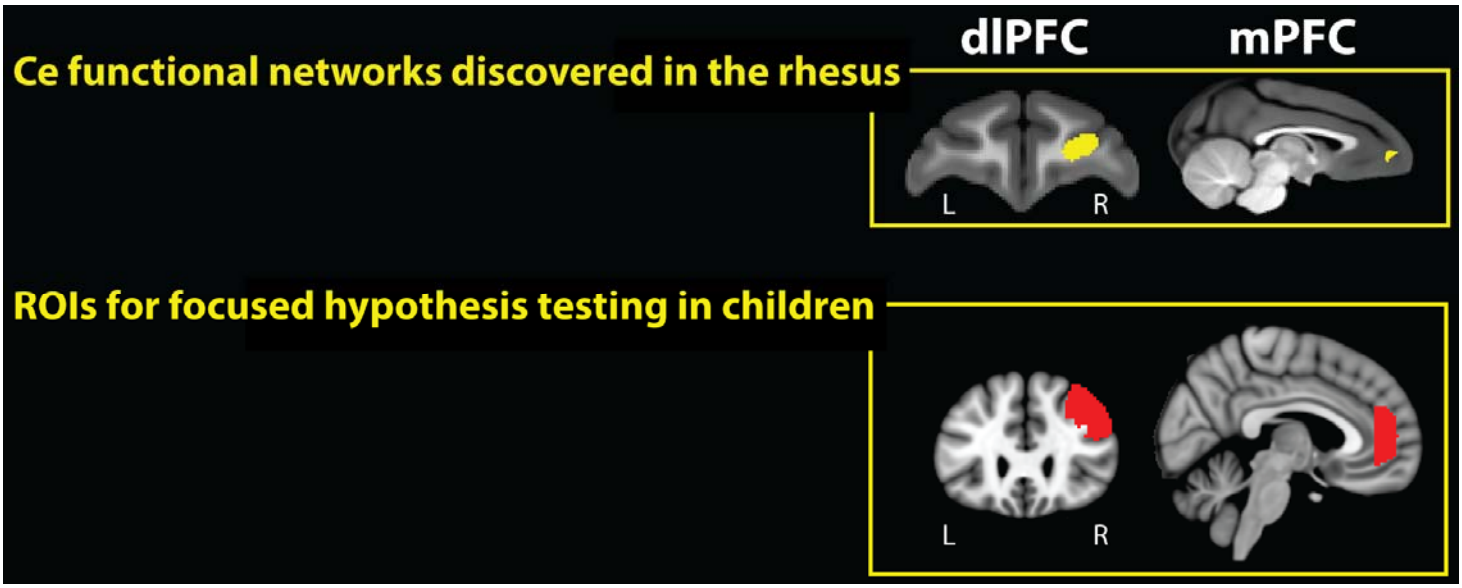

Fig. S5. The dlPFC-Ce and mPFC-Ce functional networks that were discovered in the rhesus monkey sample guided hypothesis testing in the pediatric anxiety sample. Upper row depicts the prefrontal regions (shown in yellow) where variation in Ce functional connectivity under anesthesia predicts Ce metabolism and the AT phenotype in young rhesus monkeys. Lower row depicts the corresponding regions of interest (ROIs; shown in red) used to threshold our analyses of resting functional connectivity in children (p<.05, corrected for the combined extent of both regions; 22,256 mm^3).

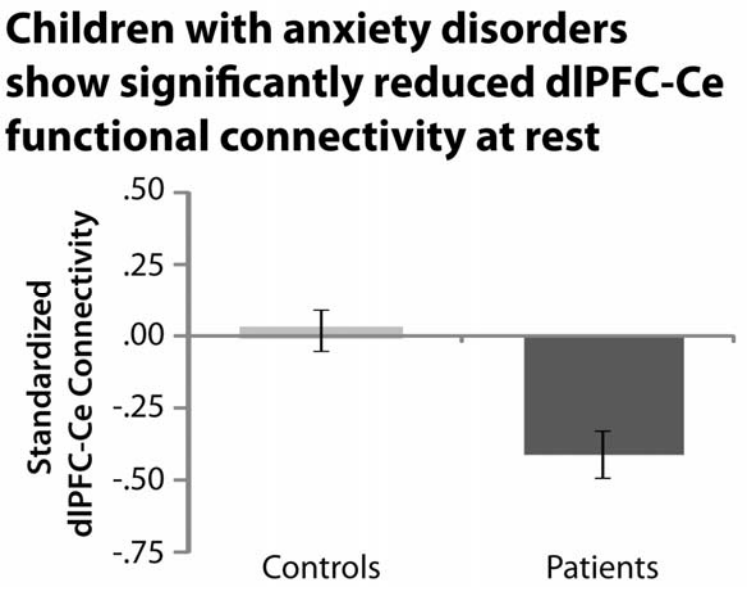

Fig. S6. Children with anxiety disorders show significantly reduced dlPFC-Ce functional connectivity at rest (*p*<.05, *df*=26, corrected for the combined volume of the medial and dorsolateral PFC; n.s., corrected for the whole brain). For illustrative purposes, the mean standardized functional connectivity for each group within the dlPFC cluster is depicted. Error bars indicate the SEM.

Continued…

SUPPLEMENTARY REFERENCES

1. Fox AS, Oakes TR, Shelton SE, Converse AK, Davidson RJ, Kalin NH. Calling for help is independently modulated by brain systems underlying goal-directed behavior and threat perception. *Proceedings of the National Academy of Sciences USA* 2005; **102:** 4176-4179.

2. Bauers KA, de Waal FBM. "Coo" vocalizations in stumptailed macaques: A controlled functional analysis. *Behaviour* 1991; **119:** 143-160.

3. Kalin NH, Shelton SE. Ontogeny and stability of separation and threat-induced defensive behaviors in rhesus monkeys during the first year of life. *Am J Primatol* 1998; **44:** 125-135.

4. Kalin NH, Shelton SE. Defensive behaviors in infant rhesus monkeys: environmental cues and neurochemical regulation. *Science* 1989; **243:** 1718-1721.

5. Oler JA, Fox AS, Shelton SE, Rogers J, Dyer TD, Davidson RJ *et al.* Amygdalar and hippocampal substrates of anxious temperament differ in their heritability. *Nature* 2010; **466:** 864-868.

6. Fox AS, Shelton SE, Oakes TR, Davidson RJ, Kalin NH. Trait-like brain activity during adolescence predicts anxious temperament in primates. *PLoS ONE* 2008; **3:** e2570.

7. Fox AS, Oler JA, Shelton SE, Nanda SA, Davidson RJ, Roseboom PH *et al.* Central amygdala nucleus (Ce) gene expression linked to increased trait-like Ce metabolism and anxious temperament in young primates. *Proc Natl Acad Sci U S A* 2012; **109:** 18108-18113.

8. Shackman AJ, Fox AS, Oler JA, Shelton SE, Davidson RJ, Kalin NH. Neural mechanisms underlying heterogeneity in the presentation of anxious temperament. *Proc Natl Acad Sci U S A* 2013; **110:** 6145-6150.

9. Tai YC, Chatziioannou A, Siegel S, Young J, Newport D, Goble RN *et al.* Performance evaluation of the microPET P4: a PET system dedicated to animal imaging. *Phys Med Biol* 2001; **46:** 1845-1862.

10. Paxinos G, Huang X, Petrides M, Toga A. *The rhesus monkey brain in stereotaxic coordinates*. 2nd edn. Academic Press: San Diego, 2009.

11. Burghy CA, Stodola DE, Ruttle PL, Molloy EK, Armstrong JM, Oler JA *et al.* Developmental pathways to amygdala-prefrontal function and internalizing symptoms in adolescence. *Nat Neurosci* 2012; **15:** 1736-1741.

12. Snyder AZ, Raichle ME. A brief history of the resting state: The Washington University perspective. *Neuroimage* 2012; **62:** 902-910.

13. Birn RM. The role of physiological noise in resting-state functional connectivity. *Neuroimage* 2012; **62:** 864-870.

14. Oler JA, Birn RM, Patriat R, Fox AS, Shelton SE, Burghy CA *et al.* Evidence for coordinated functional activity within the extended amygdala of non-human and human primates. *Neuroimage* 2012; **61:** 1059-1066.

15. Cox RW. AFNI: Software for analysis and visualization of functional magnetic resonance neuroimages. *Comput Biomed Res* 1996; **29:** 162-173.

16. Glover GH, Li TQ, Ress D. Image-based method for retrospective correction of physiological motion effects in fMRI: RETROICOR. *Magn Reson Med* 2000; **44:** 162-167.

17. Saad ZS, Glen DR, Chen G, Beauchamp MS, Desai R, Cox RW. A new method for improving functional-to-structural MRI alignment using local Pearson correlation. *Neuroimage* 2009; **44**(3)**:** 839-848.

18. Jo HJ, Saad ZS, Simmons WK, Milbury LA, Cox RW. Mapping sources of correlation in resting state FMRI, with artifact detection and removal. *Neuroimage* 2010; **52:** 571-582.

19. LaBar KS, Gitelman DR, Mesulam MM, Parrish TB. Impact of signal-to-noise on functional MRI of the human amygdala. *Neuroreport* 2001; **12:** 3461-3464.

20. Parrish TB, Gitelman DR, LaBar KS, Mesulam MM. Impact of signal-to-noise on functional MRI. *Magn Reson Med* 2000; **44:** 925-932.

21. Patriat R, Molloy EK, Meier TB, Kirk GR, Nair VA, Meyerand ME *et al.* The effect of resting condition on resting-state fMRI reliability and consistency: A comparison between resting with eyes open, closed, and fixated. *Neuroimage in press*.

22. Biswal B, Yetkin FZ, Haughton VM, Hyde JS. Functional connectivity in the motor cortex of resting human brain using echo-planar MRI. *Magn Reson Med* 1995; **34:** 537-541.

23. Fox MD, Raichle ME. Spontaneous fluctuations in brain activity observed with functional magnetic resonance imaging. *Nat Rev Neurosci* 2007; **8**(9)**:** 700-711.

24. Vincent JL, Patel GH, Fox MD, Snyder AZ, Baker JT, Van Essen DC *et al.* Intrinsic functional architecture in the anaesthetized monkey brain. *Nature* 2007; **447:** 83-86.

25. Whitfield-Gabrieli S, Ford JM. Default mode network activity and connectivity in psychopathology. *Annu Rev Clin Psychol* 2012; **8:** 49-76.

26. Hutchison RM, Everling S. Monkey in the middle: why non-human primates are needed to bridge the gap in resting-state investigations. *Front Neuroanat* 2012; **6:** 29.

27. Friston KJ. Functional and effective connectivity: A review. *Brain Connectivity* 2011; **1:** 13-36.

28. Smith SM. The future of FMRI connectivity. *Neuroimage* 2012; **62:** 1257-1266.

29. Association AP. *Diagnostic and statistical manual of mental disorders*. 4th ed., text revision edn. APA: Washington, DC, 2000.

30. Amunts K, Kedo O, Kindler M, Pieperhoff P, Mohlberg H, Shah NJ *et al.* Cytoarchitectonic mapping of the human amygdala, hippocampal region and entorhinal cortex: intersubject variability and probability maps. *Anat Embryol* 2005; **210:** 343-352.

31. Mai JK, Paxinos G, Assheuer JK. *Atlas of the human brain*. 2nd edn. Academic Press: San Diego, CA, 2004.

32. Barbas H, De Olmos J. Projections from the amygdala to basoventral and mediodorsal prefrontal regions in the rhesus monkey. *J Comp Neurol* 1990; **300**(4)**:** 549-571.

33. Amaral DG, Insausti R. Retrograde transport of D-[3H]-aspartate injected into the monkey amygdaloid complex. *Exp Brain Res* 1992; **88**(2)**:** 375-388.

34. Amaral DG, Price JL. Amygdalo-cortical projections in the monkey (Macaca fascicularis). *J Comp Neurol* 1984; **230**(4)**:** 465-496.

35. Freese JL, Amaral DG. Neuroanatomy of the primate amygdala. In: Whalen PJ, Phelps EA (eds). *The human amygdala*. Guilford: NY, 2009, pp 3-42.

36. O'Reilly JX, Croxson PL, Jbabdi S, Sallet J, Noonan MP, Mars RB *et al.* Causal effect of disconnection lesions on interhemispheric functional connectivity in rhesus monkeys. *Proc Natl Acad Sci U S A* 2013; **110**(34)**:** 13982-13987.

37. Kennedy H, Knoblauch K, Toroczkai Z. Why data coherence and quality is critical for understanding interareal cortical networks. *Neuroimage* 2013; **80:** 37-45.

Table S1. *Cluster descriptive statistics for the default mode resting state network (DM-RSN) analysis.*

Cluster	Volume (mm^3)	Regions within Cluster	Hemisphere	Association with PC seed time-series, t [a]	Local Maxima (millimeters from AC) x	y	z
Main	20268.07	FEF in the SAR (areas 6 and 8)	R	22.30	13.125	3.750	15.625
		FEF in the SAR (areas 6 and 8)	L	22.60	-11.875	3.125	15.625
		M1 (area 4)	L	18.80	-7.500	-3.125	21.250
		M1 (Area 4)	R	19.68	8.750	-3.750	21.250
		Posterior cingulate	L	82.29	-1.250	-17.500	12.500
		TPO	R	22.39	23.750	-19.375	8.750
		TPO	L	24.72	-19.375	-20.000	9.375
		MSTD	R	23.92	15.000	-23.125	10.000
		V1 extending into parahippocampal cortex	R	27.29	8.125	-23.125	0.625
		V1 extending into parahippocampal cortex	L	27.02	-6.875	-23.125	0.000
		OPt	L	27.65	-11.875	-25.625	14.375
		OPt	R	27.18	15.625	-26.250	14.375
		POa	R	23.66	10.625	-27.500	18.125
		Precuneus	R	33.75	1.875	-30.000	9.375
mPFC	10.99	Area 6M	L	16.47	0.000	12.500	17.500

[a] Regression controlling for variation in mean-centered age and sex ($p<1.6 \times 10^{-27}$, uncorrected). **Abbreviations—AC:** anterior commissure; **FEF:** frontal eye fields; **L:** left hemisphere; **M1:** primary motor cortex; **mPFC:** medial prefrontal cortex; **MSTD:** medial superior temporal area, dorsal part; **OPt:** occipital-parietal area; **PC:** posterior cingulate; **POa:** parietal-occipital area, anterior part; **R:** right hemisphere; **SAR:** superior arcuate sulcus; **TPO:** temporal-parietal-occipital area; **V1:** primary visual cortex. Regions were sorted from anterior to posterior within each cluster and labeled using Ref. (*1*), freely available at http://scalablebrainatlas.incf.org/main/coronal3d.php?template=PHT00&.

REFERENCES

1. G. Paxinos, X. Huang, M. Petrides, A. Toga, *The rhesus monkey brain in stereotaxic coordinates*. (Academic Press, San Diego, ed. 2nd, 2009).
2. J. K. Mai, G. Paxinos, T. Voss, *Atlas of the human brain*. (Academic Press, San Diego, CA, ed. 3rd, 2007)

Table S2. *Cluster descriptive statistics for the Ce resting-state network (Ce-RSN) analysis.*

Sign of Association	Cluster	Volume (mm^3)	Regions within Cluster	Hemisphere	Association with Ce seed time-series, t [a]	Local Extrema (millimeters from AC) x	y	z
Positive	Main	10052.25	mPFC (area 9/32)	L	8.93	-3.125	20.625	12.500
			mPFC (pgACC area 24a/32)	R	9.25	1.250	18.125	9.375
			mPFC (area 9/32)	R	9.65	6.875	17.500	13.125
			WM adjacent to the CS	L	9.56	-6.875	15.000	13.125
			dlPFC (area 46V)	R	9.16	16.875	11.250	11.250
			mPFC (area 6M)	L	6.70	-0.625	9.375	19.375
			dlPFC (area 9/46)	L	7.47	-13.750	9.375	11.250
			vlPFC (area 44)	R	6.88	19.375	3.125	7.500
			Insula	R	6.55	20.000	2.500	3.125
			BNST extending into the sgACC	R	14.73	5.000	1.875	3.125
			Amygdala	L	17.20	-11.875	1.250	-8.750
			Area 6	L	7.05	-13.125	1.250	11.250
			STG	R	9.11	27.500	-0.625	-6.875
			Insula	L	6.79	-19.375	-1.250	2.500
			STS	L	11.03	-21.875	-6.875	-6.875
			STG	L	7.23	-27.500	-8.750	-2.500
	Temporal	22.22	WM adjacent to Area 2/1	L	7.04	-24.375	2.500	3.125
	Posterior Temporal	98.14	TE	L	8.01	-23.125	-18.750	2.500
	Occipital	35.64	V1	R	7.46	24.375	-31.875	6.250
	Occipital	46.88	V1	L	7.67	-16.875	-38.750	-5.000
Negative	Thalamus	144.53	Pulvinar	L	-8.07	-6.250	-8.750	5.000
	Thalamus	150.15	Pulvinar	R	-9.42	8.125	-11.250	6.250
	Posterior Cingulate	82.03	Area 23	R	-8.35	1.250	-19.375	1.250

[a] Regression controlling for variation in mean-centered age and sex ($p<5.0 \times 10^{-9}$, uncorrected). **Abbreviations—AC:** anterior commissure; **BNST:** bed nucleus of the stria terminalis; **Ce:** central nucleus of the amygdala; **CS:** cingulate sulcus; **dlPFC:** dorsolateral prefrontal cortex; **L:** left hemisphere; **mPFC:** medial prefrontal cortex; **pgACC:** pregenual anterior cingulate cortex; **R:** right hemisphere; **sgACC:** subgenual anterior cingulate cortex (sgACC); **STG:** superior temporal gyrus; **STS:** superior temporal sulcus; **V1:** primary visual cortex; **vlPFC:** ventrolateral prefrontal cortex; **WM:** white matter. Regions were sorted from anterior to posterior within each cluster and labeled Ref. (*1*), freely available at http://scalablebrainatlas.incf.org/main/coronal3d.php?template=PHT00&.

REFERENCES

1. G. Paxinos, X. Huang, M. Petrides, A. Toga, *The rhesus monkey brain in stereotaxic coordinates*. (Academic Press, San Diego, ed. 2nd, 2009).
2. J. K. Mai, G. Paxinos, T. Voss, *Atlas of the human brain*. (Academic Press, San Diego, CA, ed. 3rd, 2007)

Table S3. *Cluster descriptive statistics for the association between Ce intrinsic functional connectivity and Ce metabolism.*

Cluster	Volume (mm^3)	Regions within Cluster	Hemisphere	Association with FDG, *t* [a]	Local Extrema (millimeters from AC) *x*	*y*	*z*
mPFC	378.42	FPC (area 10M) extending into OFC (area 14M) and dlPFC (area 46)	R	-4.51	3.750	26.875	7.500
		pgACC (area 32)	L	-3.82	-0.625	20.000	8.750
		dlPFC (area 46D)	L	-3.29	-11.875	13.125	11.875
dlPFC	295.41	Area 46 extending into 11, 47	R	-4.01	11.875	20.625	10.000
Occipital	309.81	V2	R	-3.97	6.875	-24.375	3.750
		V2	L	-3.89	-4.375	-25.625	6.250
Occipital	776.61	WM adjacent to V1	L	-5.02	-15.000	-27.500	4.375

[a] Regression controlling for variation in mean-centered age and sex (p<.05, whole-brain corrected). **Abbreviations—AC:** anterior commissure; **Ce:** central nucleus of the amygdala; **dlPFC:** dorsolateral prefrontal cortex; **FPC:** frontopolar cortex; **L:** left hemisphere; **mPFC:** medial prefrontal cortex; **OFC:** orbitofrontal cortex; **pgACC:** pregenual anterior cingulate cortex; **R:** right hemisphere; **V1:** primary visual cortex; **V2:** secondary visual cortex; **WM:** white matter. Regions were sorted from anterior to posterior within each cluster and labeled using Ref. (*1*), freely available at http://scalablebrainatlas.incf.org/main/coronal3d.php?template=PHT00&.

REFERENCES

1. G. Paxinos, X. Huang, M. Petrides, A. Toga, *The rhesus monkey brain in stereotaxic coordinates*. (Academic Press, San Diego, ed. 2nd, 2009).
2. J. K. Mai, G. Paxinos, T. Voss, *Atlas of the human brain*. (Academic Press, San Diego, CA, ed. 3rd, 2007)

Table S4. *Cluster descriptive statistics for the association between intrinsic Ce-PFC functional connectivity and anxious temperament (AT).*

Cluster	Volume (mm^3)	Regions within Cluster	Hemisphere	Association with AT, t [a]	Association with Ce Metabolism, t [b]	Mediation Test [c]	Local Extrema (millimeters from AC) x	y	z
mPFC	51.76	OFC (area 11) extending into OFC (area 14M), FPC (area 10M), and dlPFC (area 46)	R	-4.69	-3.53	-5.48	4.375	25.000	5.625
dlPFC	117.19	dlPFC (area 46)	R	-4.59	-3.26	-5.33	10.625	15.625	7.500
Occipital	68.60	WM adjacent to V1	L	-3.78	-4.28	-5.33	-15.625	-26.250	3.750

[a] Regression controlling for variation in mean-centered age and sex (p<.05, Sidak-corrected for the volume of the clusters where functional connectivity with the Ce significantly predicted Ce metabolism; see Table S3). [b] Regression computed using the mean functional connectivity across the entire cluster and controlling for variation in age and sex (p<.05, Sidak-corrected for the number of voxels in the three clusters). [c] Clogg's t-test (see the SI Method).
Abbreviations—AC: anterior commissure; **Ce:** central nucleus of the amygdala; **dlPFC:** dorsolateral prefrontal cortex; **FPC:** frontopolar cortex; **L:** left hemisphere; **mPFC:** medial prefrontal cortex; **OFC:** orbitofrontal cortex; **R:** right hemisphere; **V1:** primary visual cortex; **WM:** white matter. Regions were sorted from anterior to posterior within each cluster and labeled using Ref. (*1*), freely available at http://scalablebrainatlas.incf.org/main/coronal3d.php?template=PHT00&.

REFERENCES

1. G. Paxinos, X. Huang, M. Petrides, A. Toga, *The rhesus monkey brain in stereotaxic coordinates*. (Academic Press, San Diego, ed. 2nd, 2009).
2. J. K. Mai, G. Paxinos, T. Voss, *Atlas of the human brain*. (Academic Press, San Diego, CA, ed. 3rd, 2007)

Table S5. *Cluster descriptive statistics for the group difference (patients vs. controls) in intrinsic functional connectivity in children.*

Contrast	Volume (mm^3)	Regions within Cluster	Hemisphere	Patients minus Controls, *t*	Local Extrema (MNI Template) *x*	*Y*	*Z*
Patients minus Controls [a]	1040	dlPFC: IFS extending into MFG	R	-4.09	56	6	14
	448	vlPFC: IFGpo extending into iPCS [b]	R	-4.16	46	10	14
		vlPFC: aiPCS extending into iPCS [b]	R	-4.09	56	6	14
	1032	MTL: vlAmygdala extending into aHip [b]	L	4.39	-28	-4	-24
		MTL: PHG [b]	L	3.80	-36	-16	-24
	800	LOS: intersection of FG and ITG [b]	L	4.61	-44	-32	-26
	1016	Cerebellum: Crus I [b]	R	-4.98	34	-66	-34
Patients minus Controls Controlling for Age and Sex [e]	544	dlPFC: IFS extending into MFG [d]	R	-4.48	30	24	32
	728	vlPFC: IFGpo extending into iPCS [b]	R	-4.05	46	10	14
		vlPFC: aiPCS extending into iPCS [b]	R	-3.95	56	6	14
	640	MTL: vlAmygdala extending into aHip [b]	L	4.26	-28	-4	-24
		MTL: PHG [b]	L	3.55	-36	-16	-24
	968	LOS: intersection of FG and ITG [b]	L	4.66	-44	-30	-26
	928	Cerebellum: Crus I [b]	R	-5.22	36	-66	-34

[a] Whole-brain voxelwise independent *t*-test (n=14/group; p<.05 controlling for the combined volume of the dlPFC and mPFC; see the SI Method; n.s. when corrected for the volume of the whole brain). [b] Cluster fell outside of the *a priori* dlPFC/mPFC region of interest. [e] Whole-brain voxelwise independent *t*-test controlling for nuisance variance in mean-centered age and sex (n=14/group; p<.05 controlling for the approximate combined volume of the dlPFC and mPFC; see the SI Method for details).[d] Overlaps the R dlPFC cluster identified by the primary hypothesis test (*Patients minus Controls*). **Abbreviations—anterior hippocampus:** anterior hippocampus; **aiPCS:** anterior-inferior precentral sulcus; **dlPFC:** dorsolateral prefrontal cortex; **FG:** fusiform gyrus; **IFS:** intermediate frontal sulcus; **iPCS:** inferior precentral sulcus; **ITG:** inferior temporal gyrus; **L:** left hemisphere; **MFG:** middle frontal gyrus; **MTL:** medial temporal lobe; **PHG:** parahippocampal gyrus; **R:** right hemisphere; **vlPFC:** ventrolateral amygdala; **vlPFC:** ventrolateral prefrontal cortex. Clusters were labeled using a combination of the Harvard-Oxford atlases distributed with FSL (http://fsl.fmrib.ox.ac.uk) and Ref. (*2*), freely available at http://www.thehumanbrain.info.

REFERENCES

1. G. Paxinos, X. Huang, M. Petrides, A. Toga, *The rhesus monkey brain in stereotaxic coordinates*. (Academic Press, San Diego, ed. 2nd, 2009).
2. J. K. Mai, G. Paxinos, T. Voss, *Atlas of the human brain*. (Academic Press, San Diego, CA, ed. 3rd, 2007)